Eur. Phys. J. C (2024) 84:250
https://doi.org/10.1140/epjc/s10052-024-12461-x

THE EUROPEAN PHYSICAL JOURNAL C

Regular Article - Theoretical Physics

Reflected entropy for communicating black holes II: Planck braneworlds

Mir Afrasiar[3,a], **Jaydeep Kumar Basak**[1,2,b], **Ashish Chandra**[3,c], **Gautam Sengupta**[3,d]

[1] Department of Physics, National Sun Yat-Sen University, Kaohsiung 80424, Taiwan
[2] Center for Theoretical and Computational Physics, Kaohsiung 80424, Taiwan
[3] Department of Physics, Indian Institute of Technology Kanpur, Kanpur 208016, India

Received: 16 November 2023 / Accepted: 18 January 2024 / Published online: 9 March 2024
© The Author(s) 2024

Abstract We obtain the reflected entropy for bipartite mixed state configurations of two adjacent and disjoint intervals at a finite temperature in finite-sized non-gravitating reservoirs described by CFT_2s each coupled to two quantum dots at their boundaries in the large central charge limit through a replica technique. These field theory results are substantiated through a holographic computation involving the entanglement wedge cross section in the dual bulk BTZ black hole geometry truncated by two Planck branes. The two Planck branes are the holographic duals of the quantum dots described by AdS_2 slices with JT black holes. Our result reproduce the holographic duality between the reflected entropy and the bulk entanglement wedge cross section in the context of the AdS_3/CFT_2 correspondence. Subsequently we analyze the behaviour of the holographic Markov gap between the reflected entropy and the mutual information for different scenarios involving the subsystem sizes and time.

Contents

[a] e-mail: afrasiar@iitk.ac.in
[b] e-mail: jkb.hep@gmail.com
[c] e-mail: achandra@iitk.ac.in
[d] e-mail: sengupta@iitk.ac.in (corresponding author)

1 Introduction

Understanding the black hole information problem [1,2] has led to various key insights into the issue of a quantum theory of gravity. The intriguing aspect of this problem involves the fine-grained entanglement entropy of the Hawking radiation from an evaporating black hole dominating the coarse-grained thermodynamic entropy at late times which leads to a violation of unitarity. For a unitary evolution the entanglement entropy of the Hawking radiation is expected to follow the Page curve [3]. Recently, this puzzle has been investigated for toy models of quantum field theories coupled to semiclassical gravity, and a possible resolution to this issue was proposed through the "island" (quantum extremal surface) formula for the fine-grained generalized entanglement entropy of the Hawking radiation. Specifically the authors in [4,5] proposed the quantum extremal surface (QES) formula motivated by the quantum corrected Ryu-Takayanagi (RT) prescription described in [6–13]. The "island" formula emphasizes that the fine-grained generalized entanglement entropy of a subregion in quantum field theories coupled to semiclassical gravity receives contribution from regions termed entanglement island at late times.[1] It was shown in [11] that the entanglement island appears in the bulk entanglement wedge for the subregion in the QFT at late times in the context of the AdS/CFT scenario. The corresponding generalized entanglement entropy of a subregion $\mathcal{R}$ in the radiation flux of an evaporating black hole is given by

$$S[\mathcal{R}] = \min\left\{\text{ext}_{Is(\mathcal{R})}\left[\frac{\text{Area}[\partial Is(\mathcal{R})]}{4G_N} + S_{eff}[\mathcal{R}\cup Is(\mathcal{R})]\right]\right\}. \tag{1}$$

In the above equation, $Is(\mathcal{R})$ is the island region in the black hole geometry corresponding to the subregion $\mathcal{R}$.[2] The proof of the above "island" formula was provided in [125,126] through a gravitational path integral in the context of two dimensional Jackiw–Teitelboim (JT) gravity [127,128] involving saddle points described by replica wormhole configurations.

Earlier, the "island" formalism was explored in toy models of a semi-infinite non-gravitating radiation reservoir described by a CFT_2 matter field coupled to a (0+1) dimensional holographic quantum mechanical system (quantum dot) at the boundary [11,13]. The holographic dual of the quantum dot is JT gravity on a Planck brane with (1+1) dimensional conformal matter fields.[3] The non-gravitating reservoir and the Planck brane are coupled utilizing the transparent boundary conditions at the junction[11,13]. At a finite temperature, two such copies of semi-infinite CFT_2 reservoirs coupled to quantum mechanical systems at their boundaries constitute a thermo-field double (TFD) state. In this construction, the Page curve for the entanglement entropy of the radiation reservoirs was reproduced utilizing the "island" prescription.

In a generalization of the above construction, the authors in [131] considered a finite-sized non-gravitating reservoir described by CFT_2 matter field coupled to two quantum dots at their boundaries. At a finite temperature this model involves two such copies of finite sized non-gravitating radiation reservoirs characterized by CFT_2s each with quantum dots located at their boundaries. The bulk dual geometry corresponding to these quantum dots are described by two Planck branes truncating the AdS_3 space time which are AdS_2 slices involving eternal JT black holes. Transparent boundary conditions were implemented at the junctions of the Planck branes with the non gravitating radiation reser-

[1] Recently, there has been a rich development in this directions which can be found in [14–122] and the references therein.

[2] Higher dimensional generalization of the island construction for the entanglement entropy has been studied in some recent papers [17,33,39,40,123,124].

[3] An example of a quantum mechanical system (quantum dot) dual to the JT gravity is the Sachdev-Ye-Kitaev model in the infrared limit [129,130].

voirs. Subsequently, the authors computed the generalized entanglement entropy of a finite segment in both the radiation reservoirs which involves the communication of entanglement between the two eternal JT black holes on the two Planck branes.

In a different context, it is known from quantum information theory that the entanglement entropy serves as a valid entanglement measure for pure states. However the entanglement entropy is not suitable to characterize mixed state entanglement as it receives contributions from irrelevant classical and quantum correlations. This requires the introduction of other measures in quantum information theory to characterize the entanglement for mixed states. In this connection various entanglement and correlation measures were proposed to describe mixed state entanglement such as the reflected entropy, entanglement negativity, entanglement of purification amongst others in the context of quantum information theory [132–137]. Some of these measures could be explicitly computed for CFT_2 through field theory replica techniques in [136,138–142] and were substantiated through bulk holographic computations described in [136,143–157] as well. In [158], the holographic entanglement negativity for various bipartite mixed states of two adjacent and disjoint intervals in the communicating black holes model described in [131] were computed through the "island" prescription. Subsequently, analogue of the Page curves for the entanglement negativity were reproduced for different scenarios involving the subsystem sizes and time.

For the past few years the mixed state correlation measure termed the reflected entropy S_R has gained significant attention due to its holographic duality with the bulk entanglement wedge cross-section (EWCS) [136,147].[4] The reflected entropy in various models of evaporating black holes was also investigated in the context of the island construction in [30,31,52,59] and analogue of the corresponding Page curve were reproduced. In this article, we compute the reflected entropy for bipartite mixed states of two adjacent and disjoint subsystems in the model of two JT black holes communicating through finite-sized non-gravitating reservoirs [131] described earlier. Subsequently, we also obtain the holographic mutual information I for the mixed states under consideration and compare their profiles with the corresponding profiles for the holographic reflected entropy for these mixed states for various subsystem sizes and the time. The difference between these two measures characterized an important feature of multipartite entanglement termed the holographic Markov gap [166–169] in this scenario.

This article is organized as follows. In Sect. 2, we briefly review some earlier works related to our article. In Sect. 2.1 we review the model discussed in [131]. Subsequently, we provide a short review of the reflected entropy for bipartite mixed states in Sect. 2.2 in the context of the AdS/CFT scenario. Finally in the Sect. 2.3, we describe the issue of Markov gap in quantum information theory. Next, in Sect. 3, a detailed computation of the reflected entropy is described for bipartite mixed states of two adjacent and disjoint subsystems in finite-sized reservoirs each coupled to two quantum dots. Subsequently, we substantiate these field theory results from the explicit holographic computations of the bulk EWCS in the dual eternal BTZ black hole geometry. In Sect. 4, we discuss the holographic Markov gap for different scenarios of the adjacent and disjoint subsystems by comparing the corresponding profiles of the reflected entropy and the mutual information. Finally in Sect. 5, we discuss and summarize our results with some future open issues.

2 Review of earlier results

In this section, we begin with a brief review of the configuration of two JT black holes communicating through finite-sized non-gravitating reservoirs each coupled to quantum dots at their boundaries as described in [131]. The bulk dual of this configuration is described by $(2+1)$-dimensional eternal BTZ black hole geometry truncated by two Planck branes with AdS_2 geometries. The two dimensional communicating eternal JT black holes in this case are located on these Planck branes and the entire system of the black holes and the reservoirs is described by a matter CFT_2 with transparent boundary conditions at the junctions [11,13]. Subsequently, we will also review the field theory replica technique for the computation of the reflected entropy and the corresponding bulk entanglement wedge cross section in the AdS_3/CFT_2 scenario. Finally, we will discuss the emergence of the holographic Markov gap between the reflected entropy and the corresponding mutual information.

2.1 Communicating black holes

In this subsection, we describe the model of [131] and consider two eternal JT black holes at the same temperature. For this case, the bulk computation of the generalized entanglement entropy for a subsystem A described by the union of two identical intervals in the two reservoirs has been described in [158]. The Penrose diagram of the eternal JT black holes[5] located on the Planck branes is described in Fig. 1 which are coupled to each other through the shared reservoirs.

For this configuration, the metric describing the exterior regions of the two eternal JT black holes may be expressed as

$$ds_1^2 = \frac{4\pi^2}{\beta^2}\frac{-dt^2+d\xi^2}{\sinh^2\frac{2\pi\xi}{\beta}}, \quad \xi \in (-\infty, -\epsilon], \tag{2}$$

[4] For related works see also [157,159–165].

[5] The two eternal JT black holes together with the two Planck branes are labeled as a and b.

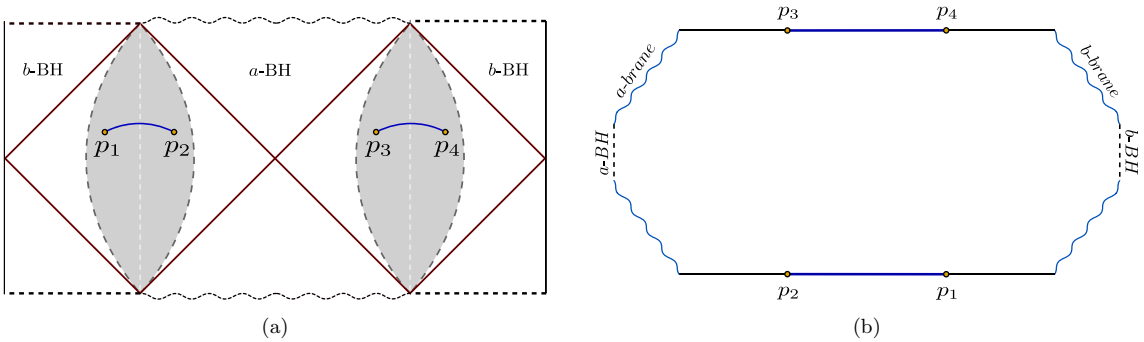

Fig. 1 Schematics depict the maximal extension of the Penrose diagram for two AdS_2 eternal black holes. The union of segments considered in the radiation reservoirs (shaded regions) describes a subsystem with the endpoints labeled as p_1, p_2, p_3, p_4. The eternal black holes located on the JT branes are denoted as a and b. (Figure modified from [131])

$$ds_2^2 = \frac{4\pi^2}{\beta^2}\frac{-dt^2+d\xi^2}{\sinh^2\frac{2\pi}{\beta}(\xi-L)}, \quad \xi\in[L+\epsilon,+\infty)\,. \tag{3}$$

The corresponding radiation reservoirs are defined by the flat metric

$$ds_R^2 = \frac{-dt^2+d\xi^2}{\epsilon^2}, \quad \xi\in[-\epsilon, L+\epsilon]\,, \tag{4}$$

where the reservoir is glued continuously to the surfaces $\xi = -\epsilon$ and $L+\epsilon$. The dilaton profiles for the two eternal JT black holes on the Planck branes are then given as follows

$$\begin{aligned}\phi_a(\xi) &= \Phi_0 + \frac{2\pi\phi_r}{\beta}\coth\frac{2\pi\xi}{\beta},\\ \phi_b(\xi) &= \Phi_0 + \frac{2\pi\phi_r}{\beta}\coth\frac{2\pi}{\beta}(\xi-L)\,.\end{aligned} \tag{5}$$

Note that here the three dimensional bulk geometry consists of an eternal BTZ black hole truncated by the two Planck branes which is described by the following metric [11,51,131]

$$ds^2 = -\frac{\left(1-\frac{z^2}{z_h^2}\right)}{z^2}dt^2 + \frac{1}{z^2\left(1-\frac{z^2}{z_h^2}\right)}dz^2 + \frac{1}{z^2}dx^2, \tag{6}$$

where the horizon at z_h is related to the inverse temperature as $\beta = 2\pi z_h$.

2.2 Reflected entropy

In this subsection we provide a brief review of the reflected entropy for the case of two disjoint subsystems as described in [136]. The authors in this work first proposed the mixed state correlation measure of the reflected entropy which involved a canonical purification of a bipartite mixed state. In this regards, consider a bipartite mixed state ρ_{AB} of disjoint subsystems A and B. The canonically purified state $|\sqrt{\rho_{AB}}\rangle$ in a doubled Hilbert space $\mathcal{H}_A\otimes\mathcal{H}_B\otimes\mathcal{H}_{A^\star}\otimes\mathcal{H}_{B^\star}$ may be constructed to purify[6] the given mixed state ρ_{AB} where $A^\star$ and $B^\star$ are the CPT conjugate copies of the subsystems A and B respectively. The reflected entropy $S_R(A:B)$ for the bipartite subsystems may be defined as [136]

$$S^R(A:B) = S_{vN}(\rho_{AA^\star})_{\sqrt{\rho_{AB}}} \tag{7}$$

where S_{vN} denotes the von Neumann entropy. In Eq. (7), the reduced density matrix $\rho_{AA^\star}$ is given by

$$\rho_{AA^\star} = \mathrm{Tr}_{\mathcal{H}_B\otimes\mathcal{H}_{B^\star}}|\sqrt{\rho_{AB}}\rangle\langle\sqrt{\rho_{AB}}|. \tag{8}$$

The authors of [136] developed a replica technique to compute the reflected entropy for bipartite mixed states in CFT_2s. For the bipartite state $|\rho_{AB}^{m/2}\rangle \equiv |\psi_m\rangle$, the replica manifold involves m-replication of the original manifold with $m\in 2\mathbb{Z}^+$. The corresponding reduced density matrix after tracing over the subsystems BB^* is then described as

$$\rho_{AA^*}^{(m)} = \mathrm{Tr}_{\mathcal{H}_B\otimes\mathcal{H}_{B^*}}|\psi_m\rangle\langle\psi_m|. \tag{9}$$

Using this reduced density matrix, the Rényi reflected entropy may now be defined as $S_n(\rho_{AA^*}^{(m)})_{\psi_m}$ which involves an nm-sheeted replica manifold with $n\in 2\mathbb{Z}$. The reflected entropy may then be obtained by implementing the replica limits $n\to 1$ and $m\to 1$ as[7]

$$S^R(A:B) = \lim_{n,m\to 1} S_n(AA^*)_{\psi_m}. \tag{10}$$

We now consider the case of the mixed state configuration of two disjoint subsystems$A\equiv[z_1,z_2]$ and $B\equiv[z_3,z_4]$ in a CFT_2. As described in [136] the reflected entropy involving

[6] For more details about the construction of the canonically purified state $|\sqrt{\rho_{AB}}\rangle$ see also [136,170].

[7] The two replica limits $n\to 1$ and $m\to 1$ do not commute with each other as discussed in [52,136,171]. In this work, we first consider $n\to 1$ and subsequently $m\to 1$ limit to compute the reflected entropy as suggested in [52,136,171].

four point twist field correlators may be obtained through the replica technique above as follows

$$S^R(A:B) = \lim_{n\to 1}\lim_{m\to 1} S_n\left(AA^*\right)_{\psi_m} = \lim_{n\to 1}\lim_{m\to 1}\frac{1}{1-n}\log \frac{\langle\sigma_{g_A}(z_1)\sigma_{g_A^{-1}}(z_2)\sigma_{g_B}(z_3)\sigma_{g_B^{-1}}(z_4)\rangle_{\text{CFT}^{\otimes mn}}}{\left(\langle\sigma_{g_m}(z_1)\sigma_{g_m^{-1}}(z_2)\sigma_{g_m}(z_3)\sigma_{g_m^{-1}}(z_4)\rangle_{\text{CFT}^{\otimes m}}\right)^n}. \tag{11}$$

Here the twist operators σ_{g_A} and σ_{g_B} are located at the endpoints of the corresponding subsystems A and B. The conformal dimensions for these twist operators are given by

$$h_{g_A^{-1}} = h_{g_B} = \frac{n\,c}{24}\left(m-\frac{1}{m}\right), \quad h_{g_Bg_A^{-1}} = \frac{2\,c}{24}\left(n-\frac{1}{n}\right), \quad h_{g_m} = \frac{c}{24}\left(m-\frac{1}{m}\right). \tag{12}$$

Following this, the authors of [31] developed a generalized version for the reflected entropy of a bipartite system AB in a holographic semi-infinite CFT_2 coupled to a semi-classical gravity which is given as follows

$$S^R_{\text{gen}}(A:B) = S^R_{\text{eff}}(A\cup \text{Is}_R(A) : B\cup \text{Is}_R(B)) + \frac{\text{Area}[Q']}{2G_N^{(2)}}, \tag{13}$$

where $Q' = \partial\text{Is}_R(A)\cap\partial\text{Is}_R(B)$. In the above expression, the first term can be computed utilizing the formula described in Eq. (10) and the second term is given by the value of the dilaton field at the island point Q' on the JT brane. In this context, since the CFT_2 located on the brane and the flat non-gravitating region is considered to be holographic, the term $S_R^{(\text{eff})}$ can be obtained from the doubly holographic perspective by computing the area of the dual EWCS in the bulk geometry as

$$S^R_{\text{gen}}(A:B) = \frac{2\text{Area(EWCS)}}{4G_N} + \frac{\text{Area}[Q']}{2G_N^{(2)}} = 2E_W(A:B) + \frac{\text{Area}[Q']}{2G_N^{(2)}}, \tag{14}$$

where we have defined $E_W(A:B) = \frac{2\text{Area(EWCS)}}{4G_N}$ in the above expression. In the following subsection, we describe the holographic Markov gap [166] as the difference between the reflected entropy and the mutual information in the framework of the AdS_3/CFT_2 correspondence.

2.3 Markov gap

In quantum information theory, the Markov gap may be described through the Markov recovery process which is defined as a recovery of the quantum state ρ_{ABC} from the bipartite mixed state ρ_{AB}. Now if we define a quantum channel $\mathcal{R}_{B\to BC}$ whose action on the bipartite mixed state ρ_{AB} produces tripartite state $\tilde{\rho}_{ABC}$ as

$$\tilde{\rho}_{ABC} = \mathcal{R}_{B\to BC}\left(\rho_{AB}\right), \tag{15}$$

where the quantum channel $\mathcal{R}$ acts on the subsystem B only. If this tripartite state $(\tilde{\rho}_{ABC})$ is equal to the quantum state ρ_{ABC} then the Markov recovery process is perfect, and the corresponding state is said to be a quantum Markov chain with the ordering $A\to B\to C$. As discussed in [172], the conditional mutual information vanishes for the perfect Markov recovery process. In this context, the authors of [173] further studied the conditional mutual information and proposed a bound in terms of the quantum Fidelity $F\left(\rho_{ABC}, \mathcal{R}_{B\to BC}\left(\rho_{AB}\right)\right)$ as

$$I(A:C\mid B) \geq -\max_{\mathcal{R}_{B\to BC}} \log F\left(\rho_{ABC}, \mathcal{R}_{B\to BC}\left(\rho_{AB}\right)\right). \tag{16}$$

Here the quantum Fidelity becomes 1 when the quantum recovery process is perfect and it becomes zero when the corresponding density matrices have support on the orthogonal subspaces. The authors of [173] also analyzed the bound in Eq. (16) for the Markov recovery process of the reduced density matrix ρ_{ABB^*} in the context of canonical purification of the subsystem B. This led to the following constraint on the conditional mutual information

$$I(A:B\mid B^*) \geq -\max_{\mathcal{R}_{B\to BB^*}} \log F\left(\rho_{ABB^*}, \mathcal{R}_{B\to BB^*}\left(\rho_{AB}\right)\right), \tag{17}$$

$$S^R(A:B) - I(A:B) \geq -\max_{\mathcal{R}_{B\to BB^*}} \log F\left(\rho_{ABB^*}, \mathcal{R}_{B\to BB^*}\left(\rho_{AB}\right)\right), \tag{18}$$

where in the last inequality, the conditional mutual information is expressed as the difference between reflected entropy and the mutual information. This difference is called as Markov gap as described in [166]. Subsequently, the authors also demonstrate that the bound in Eq. (17) may be expressed geometrically in the framework of AdS_3/CFT_2 as

$$S^R(A:B) - I(A:B) \geq \frac{\log(2)\ell_{\text{AdS}}}{2G_N} \times (\#\text{ of boundaries of EWCS }) + \mathcal{O}\left(\frac{1}{G_N}\right), \tag{19}$$

where # represents number of non-trivial boundaries of the EWCS in the bulk of AdS_3 geometry. Note that the endpoints of the EWCS located at spatial infinity does not contribute in the Eq. (19).

3 Reflected entropy and EWCS in two communicating black holes

In this section we compute the reflected entropy for various bipartite mixed states described by two adjacent and disjoint subsystems in the radiation reservoirs for the two communicating black holes configuration [131] reviewed in Sect. 2.1. In this context we first consider the adjacent subsystems in the radiation reservoirs and obtain the reflected entropy for different channels of the corresponding twist correlator in the large central charge limit. We then follow a similar analysis for the computation of the reflected entropy for two disjoint subsystems. Finally, we substantiate these field theory results from a holographic computation of the EWCS in the dual bulk geometry for these cases. Note that in the configurations (6),(7), (8) and (9) for two adjacent and disjoint subsystems, we receive an additional contribution from the dilaton term Eq. (5) in the generalized reflected entropy formula described in the Eqs. (13) and (14). However in the following section, this additional term becomes zero for other contributions since there is no QES point located on the JT brane.

3.1 Reflected entropy

3.1.1 Adjacent subsystems

We start our discussion with the computation of the reflected entropy for two adjacent subsystems $A \equiv [p_1, p_2] \cup [p_5, p_6]$ and $B \equiv [p_2, p_3] \cup [p_4, p_5]$ located in the radiation reservoirs as depicted in the figures below. To this end we utilize the replica technique developed in [136] to obtain the reflected entropy for the above bipartite mixed state for different subsystem sizes. It is observed that the reflected entropy receives contributions from various dominant channels of the corresponding twist correlators in the large central charge limit. In what follows we compute these contributions to the reflected entropy for different configurations described by the relative subsystem sizes for the communicating black hole setup as shown in Fig. 1.

Configuration-1

We begin with the computation of the reflected entropy for the contribution as described in Fig. 2a where the twist operators are located at the endpoints of the two adjacent subsystems and the Planck branes where the entire black hole/reservoir setup is described by the same CFT_2. The Rényi reflected entropy for this configuration may be obtained from the following twist correlator

$$S^R_{n,m}(A:B) = 2\frac{1}{1-n} \log \frac{\langle \sigma_{g_B^{-1}}(a_1)\sigma_{g_A}(p_1)\sigma_{g_Bg_A^{-1}}(p_2)\sigma_{g_B^{-1}}(p_3)\sigma_{g_B}(b_1)\rangle_{\text{CFT}^{\otimes mn}}}{\langle \sigma_{g_m^{-1}}(a_1)\sigma_{g_m}(p_1)\sigma_{g_m^{-1}}(p_3)\sigma_{g_m}(b_1)\rangle^n_{\text{CFT}^{\otimes m}}}, \tag{20}$$

where the points a_1 and b_1 are located on the a and b-branes respectively. In the above equation, the factor two correspond to the contribution of the reflected entropy from the TFD copy of the radiation reservoir. Note that the correlator in Eq. (20) factorizes into the respective contractions in the large central charge limit as follows [31]

$$S^R_{n,m}(A:B) = 2\frac{1}{1-n} \log \frac{\langle \sigma_{g_B^{-1}}(a_1)\sigma_{g_A}(p_1)\sigma_{g_Bg_A^{-1}}(p_2)\rangle_{\text{CFT}^{\otimes mn}}\langle \sigma_{g_B^{-1}}(p_3)\sigma_{g_B}(b_1)\rangle_{\text{CFT}^{\otimes mn}}}{\left(\langle \sigma_{g_m^{-1}}(a_1)\sigma_{g_m}(p_1)\rangle_{\text{CFT}^{\otimes m}}\langle \sigma_{g_m^{-1}}(p_3)\sigma_{g_m}(b_1)\rangle_{\text{CFT}^{\otimes m}}\right)^n}. \tag{21}$$

In this case the dominant contribution to the Rényi reflected entropy arises from the correlator

$$S^R_{n,m}(A:B) = 2\frac{1}{1-n} \log \frac{\langle \sigma_{g_B^{-1}}(a_1)\sigma_{g_A}(p_1)\sigma_{g_Bg_A^{-1}}(p_2)\rangle_{\text{CFT}^{\otimes mn}}}{\left(\langle \sigma_{g_m^{-1}}(a_1)\sigma_{g_m}(p_1)\rangle_{\text{CFT}^{\otimes m}}\right)^n} \tag{22}$$

which may be obtained following the analysis described in [31]. In the replica limit ($n \to 1$ and $m \to 1$) the reflected entropy is then given from the above equation as follows

$$S^R_{\text{eff}}(A:B) = \frac{2c}{3} \log\left[4\frac{\sinh\frac{\pi(p_2-p_1)}{\beta}\sinh\frac{\pi(a_1+p_2)}{\beta}}{\sinh\frac{\pi(a_1+p_1)}{\beta}\sinh\frac{\pi(\epsilon)}{\beta}}\right], \tag{23}$$

where ϵ is the UV cutoff in the CFT_2.

Configuration-2

In this case, the computation of the reflected entropy for the two adjacent subsystems is similar to configuration-1, however, the factorization of the twist correlator in Eq. (20) in the large central charge limit is different due to the change in the size of the subsystems A and B as shown in Fig. 2b which alters the location of the relevant twist operators. In this case the Rényi reflected entropy is given by the following expression

$$S^R_{n,m}(A:B) = 2\frac{1}{1-n} \log \frac{\langle \sigma_{g_B^{-1}}(a_1)\sigma_{g_A}(p_1)\rangle_{\text{CFT}^{\otimes mn}}\langle \sigma_{g_Bg_A^{-1}}(p_2)\sigma_{g_B^{-1}}(p_3)\sigma_{g_B}(b_1)\rangle_{\text{CFT}^{\otimes mn}}}{\left(\langle \sigma_{g_m^{-1}}(a_1)\sigma_{g_m}(p_1)\rangle_{\text{CFT}^{\otimes m}}\langle \sigma_{g_m^{-1}}(p_3)\sigma_{g_m}(b_1)\rangle_{\text{CFT}^{\otimes m}}\right)^n}, \tag{24}$$

where the factor two in the above expression arises from the reservoir copy of the double TFD states. Finally we obtain the dominant contribution to the Rényi reflected entropy in this configuration as follows

$$S^R_{n,m}(A:B) = 2\frac{1}{1-n} \log \frac{\langle \sigma_{g_B g_A^{-1}}(p_2)\sigma_{g_B^{-1}}(p_3)\sigma_{g_B}(b_1)\rangle_{CFT^{\otimes mn}}}{\left(\langle \sigma_{g_m^{-1}}(p_3)\sigma_{g_m}(b_1)\rangle_{CFT^{\otimes m}}\right)^n}, \tag{25}$$

which involves the points p_2, p_3 and b_1 after the factorization in the large central charge limit. The final expression for the reflected entropy in the replica limit following [31,136] is then given as

$$S^R_{\text{eff}}(A:B) = \frac{2c}{3}\log\left[4\frac{\sinh\frac{\pi(p_3-p_2)}{\beta}\sinh\frac{\pi(b_1+p_2)}{\beta}}{\sinh\frac{\pi(b_1+p_3)}{\beta}\sinh\frac{\pi(\epsilon)}{\beta}}\right], \tag{26}$$

where ϵ is the CFT_2 UV cutoff.

Configuration- 3 and 4

These configurations are depicted in the Fig. 2c and d and the computation of the reflected entropy for these cases is similar to the configurations 1 and 2. Here, the dominant contributions for the configuration-3 and 4 are given by the Eqs. (22) and (25) in the large central charge limit. Note that the only difference in these configurations arise due to the locations of the twist operators at the points p_3 and p_6 for the configuration-3 while the other configuration involves the points p_1 and p_4. However, these twist correlators cancel from the numerator and the denominator in the computation of the reflected entropy in the replica limit. Hence the reflected entropy for the configuration-3 is given by Eq. (23) and similarly Eq. (26) provides the result for the configuration-4.

Configuration- 5

The computation of the reflected entropy for this configuration as depicted in Fig. 2e is trivial since it reduces to the analysis for the reflected entropy for two adjacent subsystems in a standard CFT_2. Hence the reflected entropy may be obtained for this case as follows

$$S^R(A:B) = \frac{2c}{3}\log\left[4\frac{\sinh\frac{\pi(p_3-p_2)}{\beta}\sinh\frac{\pi(p_3-p_2)}{\beta}}{\sinh\frac{\pi(p_3-p_1)}{\beta}\sinh\frac{\pi(\epsilon)}{\beta}}\right]. \tag{27}$$

Configuration-6

In this configuration the nontrivial contribution to the reflected entropy arises from the twist correlators involving the QES point a_2 on the a-brane and the point p_2 in the reservoir as depicted in Fig. 3a. There is also an additional contribution from the Weyl factor involving the point a_2 while the Weyl factors associated with the coincident points a_1 and b_1 cancels from the numerator and the denominator in the expression for the reflected entropy. Hence the Rényi reflected entropy for this configuration is given as follows

$$S^R_{n,m}(A:B) = 2\frac{1}{1-n} \log \frac{\langle \sigma_{g_B^{-1}g_A}(a_2)\sigma_{g_A^{-1}}(a_1)\sigma_{g_A}(p_1)\sigma_{g_B g_A^{-1}}(p_2)\sigma_{g_B^{-1}}(p_3)\sigma_{g_B}(b_1)\rangle_{CFT^{\otimes mn}}}{\langle \sigma_{g_m^{-1}}(a_1)\sigma_{g_m}(p_1)\sigma_{g_m^{-1}}(p_3)\sigma_{g_m}(b_1)\rangle^n_{CFT^{\otimes m}}}. \tag{28}$$

The correlator in Eq. (28) factorizes in the large central charge limit as follows

$$S^R_{n,m}(A:B) = 2\frac{1}{1-n} \log \frac{\left\langle \sigma_{g_A^{-1}}(a_1)\sigma_{g_A}(p_1)\right\rangle\left\langle \sigma_{g_B^{-1}g_A}(a_2)\sigma_{g_B g_A^{-1}}(p_2)\right\rangle\left\langle \sigma_{g_B^{-1}}(p_3)\sigma_{g_B}(b_1)\right\rangle}{\left(\left\langle \sigma_{g_m^{-1}}(a_1)\sigma_{g_m}(p_1)\right\rangle\left\langle \sigma_{g_m^{-1}}(p_3)\sigma_{g_m}(b_1)\right\rangle\right)^n}. \tag{29}$$

Note that the correlators in the numerator and denominator of Eq. (29) are defined in the mn and m replicated sheets respectively. The dominant contribution to the Rényi reflected entropy in this case then arises from the correlator involving the points a_2 and p_2 in the large central charge limit as follows

$$S^R_{n,m}(A:B) = 2\frac{1}{1-n}\log\langle \sigma_{g_B^{-1}g_A}(a_2)\sigma_{g_B g_A^{-1}}(p_2)\rangle_{CFT^{\otimes mn}}. \tag{30}$$

Finally the reflected entropy for this configuration may be obtained in the replica limit as

$$S^R_{\text{eff}}(A:B) = \frac{2c}{3}\log\left[\frac{\beta}{\pi}\frac{\cosh\left(\frac{2\pi(a_2-p_2)}{\beta}\right)-1}{\sinh\left(\frac{2\pi a_2}{\beta}\right)}\right]. \tag{31}$$

Now we may obtain the generalized reflected entropy utilizing the island formula in Eq. (13) as follows

$$S^R_{\text{gen}}(A:B) = 2\Phi_0 + \frac{4\pi\Phi_r}{\beta}\coth\left(\frac{2\pi a_2}{\beta}\right) + \frac{2c}{3}\log\left[\frac{\beta}{\pi}\frac{\cosh\left(\frac{2\pi(a_2-p_2)}{\beta}\right)-1}{\sinh\left(\frac{2\pi a_2}{\beta}\right)}\right]. \tag{32}$$

Configuration-7

This configuration is similar to the configuration-6, however, the reflected entropy in this case receives contribution from the QES point b_2 located on the b-brane. Hence, the twist correlator for the Rényi reflected entropy factorizes to the following contraction in the large central large limit

$$S^R_{n,m}(A:B) = 2\frac{1}{1-n} \log \frac{\left\langle \sigma_{g_A^{-1}}(a_1)\sigma_{g_A}(p_1)\right\rangle\left\langle \sigma_{g_B^{-1}g_A}(b_2)\sigma_{g_B g_A^{-1}}(p_2)\right\rangle\left\langle \sigma_{g_B^{-1}}(p_3)\sigma_{g_B}(b_1)\right\rangle}{\left(\left\langle \sigma_{g_m^{-1}}(a_1)\sigma_{g_m}(p_1)\right\rangle\left\langle \sigma_{g_m^{-1}}(p_3)\sigma_{g_m}(b_1)\right\rangle\right)^n}, \tag{33}$$

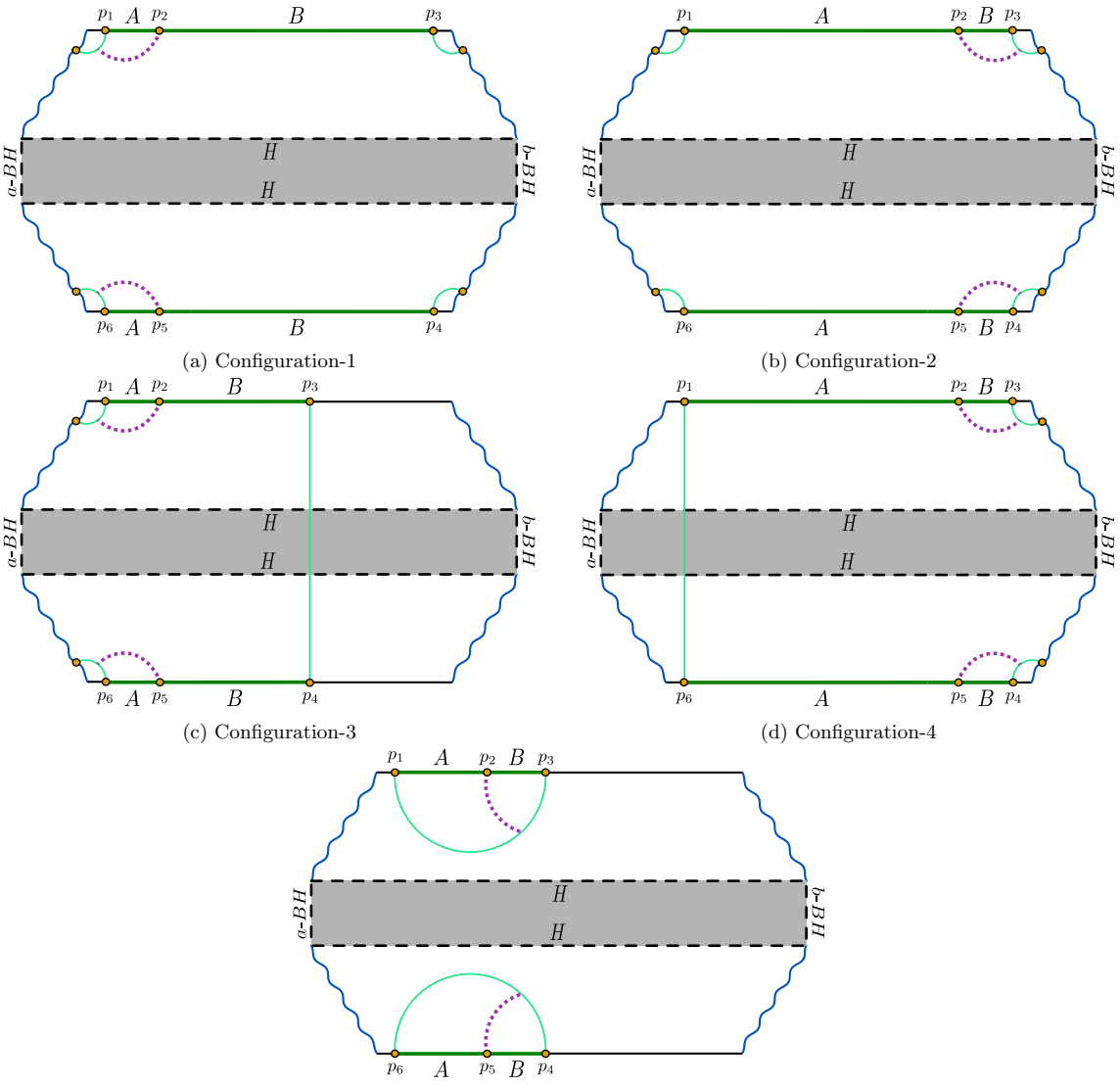

(a) Configuration-1 (b) Configuration-2

(c) Configuration-3 (d) Configuration-4

(e) Configuration-5

Fig. 2 Schematics depicts all the possible contributions to the reflected entropy for the case of two adjacent subsystems A and B where we get connected phase of entanglement island for initial four phases only

where the dominant contribution in the above equation involves twist operators located at the points b_2 and p_2 as shown in Fig. 3b. Thus the Rényi reflected entropy is given by the following equation

$$S^R_{n,m}(A:B) = 2\frac{1}{1-n}\log\langle\sigma_{g_B^{-1}g_A}(b_2)\sigma_{g_Bg_A^{-1}}(p_2)\rangle_{\text{CFT}^{\otimes mn}}\,. \tag{34}$$

Finally, the expression of the reflected entropy may be obtained in the replica limit as follows

$$S^R_{\text{eff}}(A:B) = \frac{2c}{3}\log\left[\frac{\beta}{\pi}\frac{\cosh\left(\frac{2\pi(b_2-p_2)}{\beta}\right)-1}{\sinh\left(\frac{2\pi b_2}{\beta}\right)}\right]. \tag{35}$$

For this configuration, we may now obtain the generalized reflected entropy by using the island formula in Eq. (13) as

$$S^R_{\text{gen}}(A:B) = 2\Phi_0 + \frac{4\pi\Phi_r}{\beta}\coth\left(\frac{2\pi(L-b_2)}{\beta}\right) + \frac{2c}{3}\log\left[\frac{\beta}{\pi}\frac{\cosh\left(\frac{2\pi(b_2-p_2)}{\beta}\right)-1}{\sinh\left(\frac{2\pi b_2}{\beta}\right)}\right]. \tag{36}$$

Configuration-8 and 9

The computation of the reflected entropy in this cases follow the analysis described for the configurations-6 and 7. The dominant contributions in these cases are then given by Eqs. (30) and (34) in the large central charge limit. The

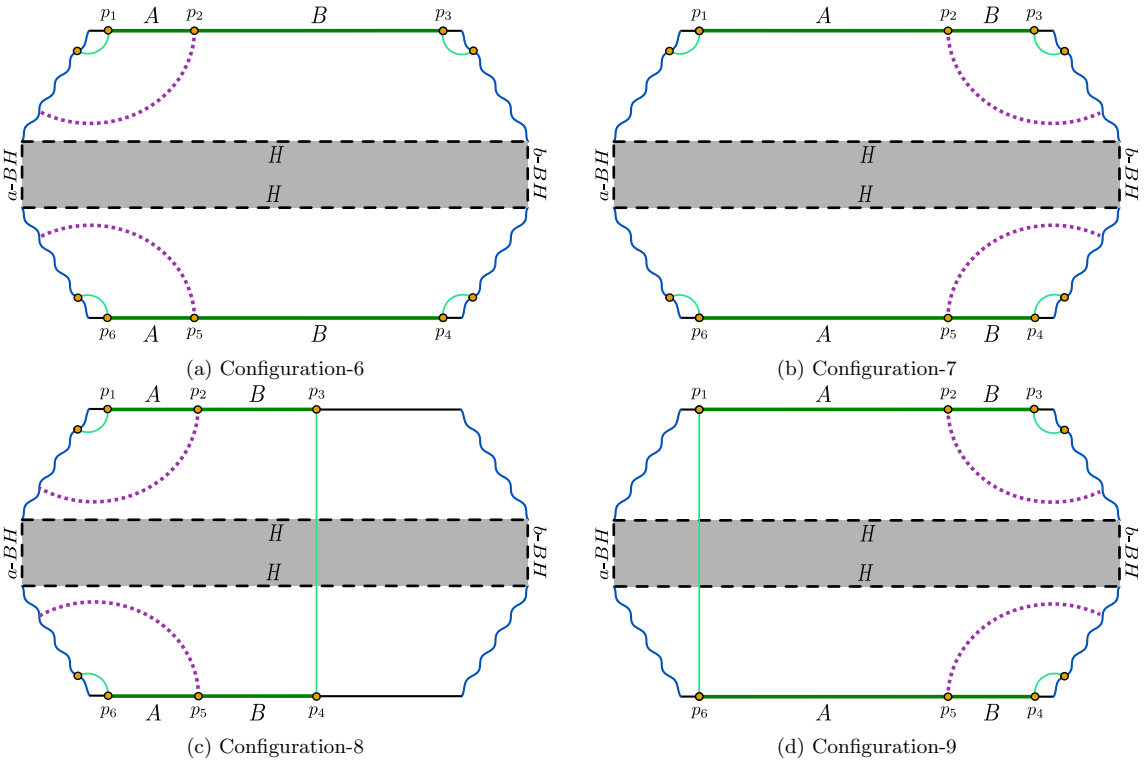

(a) Configuration-6 (b) Configuration-7

(c) Configuration-8 (d) Configuration-9

Fig. 3 The non-trivial cross section in each of the following channels for the reflected entropy is shown with a connected phase of the entanglement island

only difference between these two configurations arise from the location of the twist operators at points p_3 and p_6 as depicted in Fig. 3c for the first while the other configuration 3d incorporate twist operators located at the points p_1 and p_4. However, the contribution from these correlators cancel in the replica limit. Therefore the reflected entropy for the configuration-8 is given by the Eq. (32) and similarly the Eq. (36) describes the result for the configuration- 9.

Configuration-10

Now we describe the next configuration where the reflected entropy involves contribution from the points located on both the radiation reservoirs as depicted in the Fig. 4a. In this case, the Weyl factors cancel from the numerator and denominator in the reflected entropy expression in the replica limit. Hence the Rényi reflected entropy for this configuration is given by

$$S^R_{n,m}(A:B)=\frac{1}{1-n}\log\left[\frac{\left\langle\sigma_{g_A^{-1}}(a_1)\sigma_{g_A}(p_1)\sigma_{g_Bg_A^{-1}}(p_2)\sigma_{g_B^{-1}}(p_3)\sigma_{g_B}(b_1)\right.}{\left\langle\sigma_{g_m^{-1}}(a_1)\sigma_{g_m}(p_1)\sigma_{g_m^{-1}}(p_3)\sigma_{g_m}(b_1)\right.}\frac{\left.\sigma_{g_A^{-1}}(a_2)\sigma_{g_A}(p_4)\sigma_{g_Bg_A^{-1}}(p_5)\sigma_{g_B^{-1}}(p_6)\sigma_{g_B}(b_2)\right\rangle_{\mathrm{CFT}^{\otimes mn}}}{\left.\sigma_{g_m^{-1}}(a_2)\sigma_{g_m}(p_4)\sigma_{g_m^{-1}}(p_5)\sigma_{g_m}(b_2)\right\rangle^n_{\mathrm{CFT}^{\otimes m}}}\right]. \tag{37}$$

In the large central charge limit, the above expression factorizes to the following contractions

$$S^R_{n,m}(A:B)=\frac{1}{1-n}\log\left[\frac{\left\langle\sigma_{g_A^{-1}}(a_1)\sigma_{g_A}(p_1)\right\rangle\left\langle\sigma_{g_Bg_A^{-1}}(p_2)\sigma_{g_Bg_A^{-1}}(p_5)\right\rangle\left\langle\sigma_{g_B^{-1}}(p_3)\sigma_{g_B}(b_1)\right\rangle}{\left(\left\langle\sigma_{g_m^{-1}}(a_1)\sigma_{g_m}(p_1)\right\rangle\left\langle\sigma_{g_m^{-1}}(p_3)\sigma_{g_m}(b_1)\right\rangle\right)^n}\frac{\left\langle\sigma_{g_A^{-1}}(a_2)\sigma_{g_A}(p_4)\right\rangle\left\langle\sigma_{g_B^{-1}}(p_6)\sigma_{g_B}(b_2)\right\rangle}{\left(\left\langle\sigma_{g_m^{-1}}(a_2)\sigma_{g_m}(p_4)\right\rangle\left\langle\sigma_{g_m^{-1}}(p_6)\sigma_{g_m}(b_2)\right\rangle\right)^n}\right]. \tag{38}$$

Now the reflected entropy in this configuration may be obtained from the dominant correlator involving the twist operators located at the points p_2 and p_5 since the other correlators in Eq. (38) cancel from the numerator and denominator in the replica limit. Hence, the Rényi reflected entropy reduced to the following expression

$$S^R_{n,m}(A:B) = \frac{1}{1-n}\log\left\langle \sigma_{g_B g_A^{-1}}(p_2)\sigma_{g_B g_A^{-1}}(p_5)\right\rangle. \tag{39}$$

Note that the correlator involving twist operators from the TFD copies of the CFT_2s are also studied in the article [174]. Finally, we may obtain the reflected entropy as follows

$$S^R_{\text{eff}}(A:B) = \frac{2c}{3}\log\left[\frac{\beta}{\pi}\cosh\left(\frac{2\pi t}{\beta}\right)\right]. \tag{40}$$

Configuration-11 and 12

In these configurations, the computation of the reflected entropy for two adjacent subsystems A and B also follow the similar analysis described in configuration-10, and the dominant correlators in these cases are given by the Eq. (39). Therefore apart from the change in the factorization of the correlators in these configurations as depicted in Fig. 4b and c, the results of the reflected entropies remain identical, which is given by Eq. (40).

Configuration-13

In this case, the Rényi reflected entropy of two adjacent subsystems A and B involves twist operators located on both the radiation reservoirs as depicted in Fig. 5a and the dominant contribution arises from the the four point twist field correlator in the computation for the reflected entropy. For this configuration, the Rényi reflected entropy may be obtained from the following expression

$$S^R_{n,m}(A:B) = \frac{1}{1-n}\log\left[\frac{\left\langle \sigma_{g_A^{-1}}(a_1)\sigma_{g_A}(p_1)\sigma_{g_B g_A^{-1}}(p_2)\sigma_{g_B^{-1}}(p_3)\sigma_{g_A^{-1}}(a_2)\right\rangle}{\left\langle \sigma_{g_m^{-1}}(a_1)\sigma_{g_m}(p_1)\sigma_{g_m^{-1}}(p_3)\right\rangle}\frac{\left\langle \sigma_{g_A}(p_4)\sigma_{g_B g_A^{-1}}(p_5)\sigma_{g_B^{-1}}(p_6)\right\rangle_{\text{CFT}^{\otimes mn}}}{\left\langle \sigma_{g_m^{-1}}(a_2)\sigma_{g_m}(p_4)\sigma_{g_m^{-1}}(p_6)\right\rangle^n_{\text{CFT}^{\otimes m}}}\right], \tag{41}$$

where the correlator does not involve any QES point on the b-brane. The factorization of the above correlator in the large central charge limit implies the following expression of the Rényi reflected entropy

$$S^R_{n,m}(A:B) = \frac{1}{1-n}\log\left[\frac{\left\langle \sigma_{g_A^{-1}}(a_1)\sigma_{g_A}(p_1)\right\rangle\left\langle \sigma_{g_B g_A^{-1}}(p_2)\sigma_{g_B^{-1}}(p_3)\sigma_{g_B g_A^{-1}}(p_5)\sigma_{g_B^{-1}}(p_6)\right\rangle}{\left(\left\langle \sigma_{g_m^{-1}}(a_1)\sigma_{g_m}(p_1)\right\rangle\left\langle \sigma_{g_m^{-1}}(p_3)\sigma_{g_m^{-1}}(p_6)\right\rangle\right)^n}\frac{\left\langle \sigma_{g_A^{-1}}(a_2)\sigma_{g_A}(p_4)\right\rangle}{\left(\left\langle \sigma_{g_m^{-1}}(a_2)\sigma_{g_m}(p_4)\right\rangle\right)^n}\right]. \tag{42}$$

In the above equation, the dominant correlator involves twist operators located at the points p_2, p_3, p_4 and p_5 while the other contributions cancel from the nominator and denominator in Eq. (42). Hence the Rényi reflected entropy reduced to the following form

$$S^R_{n,m}(A:B) = \frac{1}{1-n}\times\log\frac{\left\langle \sigma_{g_B g_A^{-1}}(p_2)\sigma_{g_B^{-1}}(p_3)\sigma_{g_B g_A^{-1}}(p_5)\sigma_{g_B^{-1}}(p_6)\right\rangle}{\left(\left\langle \sigma_{g_m^{-1}}(p_3)\sigma_{g_m^{-1}}(p_6)\right\rangle\right)}. \tag{43}$$

Now, we utilize a technique termed as inverse doubling trick described in [175] to compute the reflected entropy from Eq. (43). In this trick, the four point twist correlator is reduced to the two point function in the $BCFT_2$, and we can obtain the expression of this two point twist correlator in the OPE channel by following the analysis described in [175]. Finally, the reflected entropy in the replica limit may be computed as

$$S^R_{\text{eff}}(A:B) = \frac{2c}{3}\times\log\left[\frac{(r_3-r_2)\,\text{sech}\left(\frac{2\pi t}{\beta}\right)\sqrt{r_3^2+2r_3r_2\cosh\left(\frac{4\pi t}{\beta}\right)+r_2^2}}{r_3\epsilon}\right], \tag{44}$$

where r_3 and r_2 are the location of the points p_3 and p_2 respectively.

Configuration-14

This case is similar to the configuration-13 as shown in Fig. 5b, and the twist field correlator for the Rényi reflected entropy factorizes in the following contraction in the large central charge limit

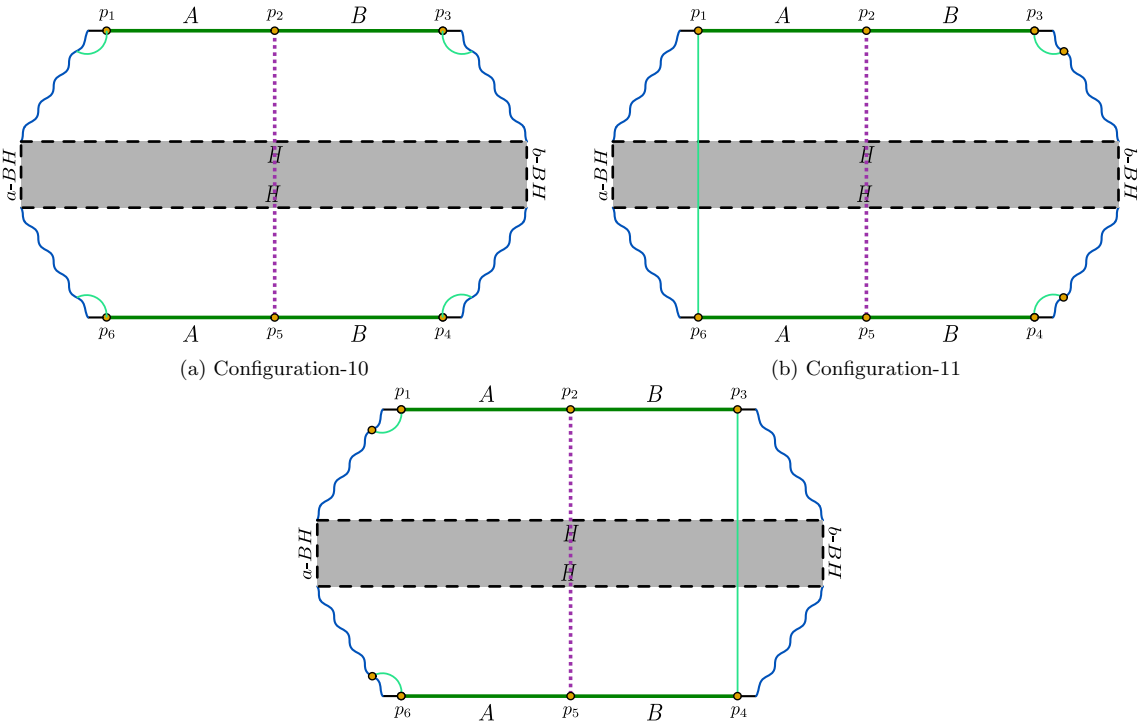

(a) Configuration-10 (b) Configuration-11

(c) Configuration-12

Fig. 4 The corresponding figures depict the connected phase of the entanglement island with non-trivial cross section extending between the TFD copies of the radiation reservoirs

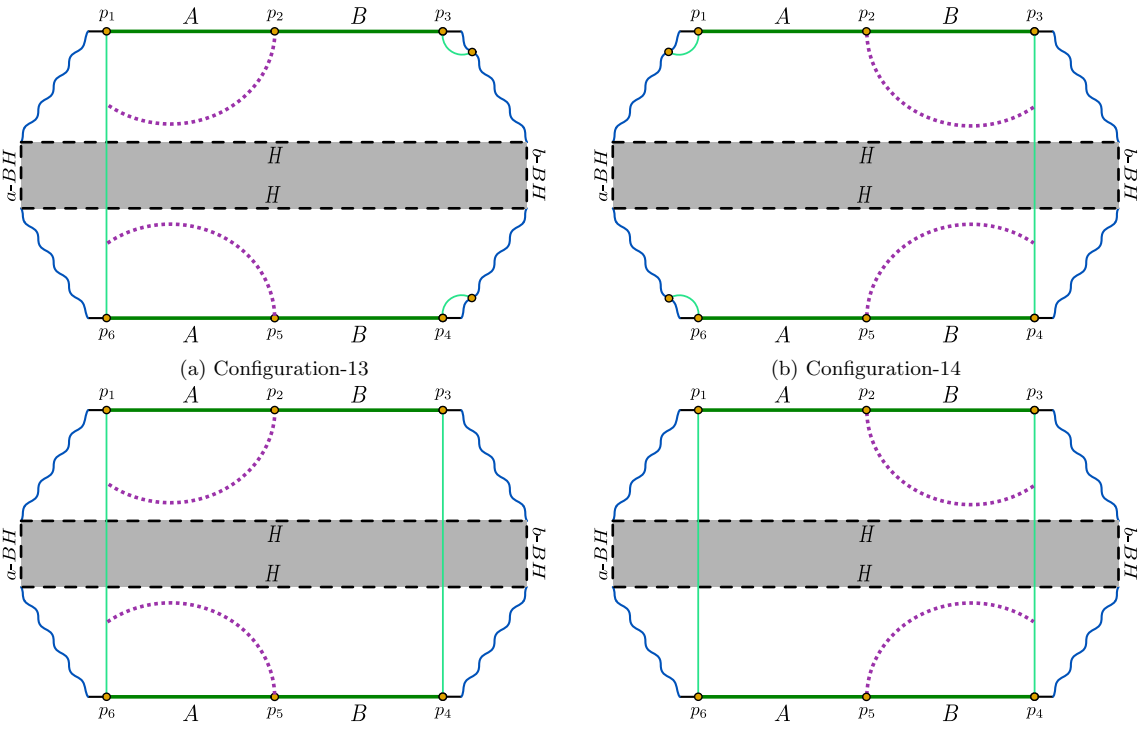

(a) Configuration-13 (b) Configuration-14

(c) Configuration-15 (d) Configuration-16

Fig. 5 Schematics depicts the non-trivial cross section to the reflected entropy of the two adjacent subsystems A and B where the corresponding cross section ended of the Hartman-Maldacena surface

$$S^R_{n,m}(A:B)=\frac{1}{1-n}\log\left[\frac{\left\langle\sigma_{g_A^{-1}}(b_1)\sigma_{g_B^{-1}}(p_3)\right\rangle\left\langle\sigma_{g_A}(p_1)\sigma_{g_Bg_A^{-1}}(p_2)\sigma_{g_Bg_A^{-1}}(p_4)\sigma_{g_B^{-1}}(p_5)\right\rangle}{\left(\left\langle\sigma_{g_m^{-1}}(b_1)\sigma_{g_m}(p_3)\right\rangle\left\langle\sigma_{g_m^{-1}}(p_1)\sigma_{g_m^{-1}}(p_5)\right\rangle\right)^n}\frac{\left\langle\sigma_{g_A^{-1}}(b_2)\sigma_{g_A}(p_6)\right\rangle}{\left(\left\langle\sigma_{g_m^{-1}}(b_2)\sigma_{g_m}(p_6)\right\rangle\right)^n}\right]. \quad (45)$$

The dominant correlator in Eq. (45) involves twist operators located at the points p_1, p_2, p_4 and p_5 while the other contributions cancel from the nominator and denominator in the replica limit. Hence the Rényi reflected entropy may be reduced as

$$S^R_{n,m}(A:B)=\frac{1}{1-n}\log\frac{\left\langle\sigma_{g_A}(p_1)\sigma_{g_Bg_A^{-1}}(p_2)\sigma_{g_Bg_A^{-1}}(p_4)\sigma_{g_B^{-1}}(p_5)\right\rangle}{\left(\left\langle\sigma_{g_m^{-1}}(p_1)\sigma_{g_m^{-1}}(p_5)\right\rangle\right)^n}. \quad (46)$$

On utilization of the techniques discussed in [136,175], the reflected entropy may be obtained as follows

$$S^R_{\text{eff}}(A:B)=\frac{2c}{3}\times\log\left[\frac{(r_1-r_2)\,\text{sech}\left(\frac{2\pi t}{\beta}\right)\sqrt{r_1^2+2r_1r_2\cosh\left(\frac{4\pi t}{\beta}\right)+r_2^2}}{r_1\epsilon}\right], \quad (47)$$

where r_1 and r_2 are location of the points p_1 and p_2 respectively.

Configuration-15 and 16

In these configurations, the computation of the reflected entropy for two adjacent subsystems A and B follows a similar analysis as described for the configurations-13 and 14. Here the dominant correlators for the configurations-15 and 16 are given by the Eqs. (43) and (46) respectively in the large central charge limit. The only difference in these configurations arise from the twist operators located at the points p_1 and p_4 as depicted in Fig. 5c for the first, while the other configuration Fig. 5d involves twist operators located at the points p_3 and p_6. However the contributions from these two point twist correlators cancel from the numerator and denominator in the replica limit. Hence the expression for the reflected entropies in the configurations-15 and 16 are given by Eqs. (44) and (47) respectively.

3.1.2 Disjoint subsystems

In this subsection, we discuss the computation of the reflected entropy for two disjoint subsystems $A\equiv[p_1,p_2]\cup[p_5,p_6]$ and $B\equiv[p_3,p_4]\cup[p_7,p_8]$ located on both the radiation reservoirs described by CFT_2s in the communicating black hole setup as shown in Fig. 1. In this context we obtain the reflected entropy for different configurations described by relative subsystem sizes utilizing the techniques developed in [136].

Configuration-1

We first discuss the configuration which involves the twist operators located on the radiation reservoirs and the a, b-branes as depicted in Fig. 6a. Since this configuration is symmetric on the reservoir copy of the double TFD states it suffices to compute the reflected entropy of the two disjoint subsystems in one of the reservoirs. Hence the Rényi reflected entropy may be obtained using the following twist correlator

$$S^R_{n,m}(A:B)=2\frac{1}{1-n}\log\frac{\langle\sigma_{g_B^{-1}}(a_1)\sigma_{g_A}(p_1)\sigma_{g_A^{-1}}(p_2)\sigma_{g_B}(p_3)\sigma_{g_B^{-1}}(p_4)\sigma_{g_B}(b_1)\rangle_{\text{CFT}^{\otimes mn}}}{\langle\sigma_{g_m^{-1}}(a_1)\sigma_{g_m}(p_1)\sigma_{g_m^{-1}}(p_2)\sigma_{g_m}(p_3)\sigma_{g_m^{-1}}(p_4)\sigma_{g_m}(b_1)\rangle^n_{\text{CFT}^{\otimes m}}}, \quad (48)$$

where the factor 2 in the above equation incorporates the contribution to the reflected entropy from the other copy of the radiation reservoir. In the large central charge limit, the correlators in Eq. (48) factorize to the respective contractions as follows

$$S^R_{n,m}(A:B)=2\frac{1}{1-n}\log\left[\frac{\langle\sigma_{g_B^{-1}}(a_1)\sigma_{g_A}(p_1)\sigma_{g_A^{-1}}(p_2)\sigma_{g_B}(p_3)\rangle_{\text{CFT}^{\otimes mn}}}{\left(\langle\sigma_{g_m^{-1}}(a_1)\sigma_{g_m}(p_1)\sigma_{g_m^{-1}}(p_2)\sigma_{g_m}(p_3)\rangle_{\text{CFT}^{\otimes m}}\right)^n}\frac{\langle\sigma_{g_B^{-1}}(p_4)\sigma_{g_B}(b_1)\rangle_{\text{CFT}^{\otimes mn}}}{\left(\langle\sigma_{g_m^{-1}}(p_4)\sigma_{g_m}(b_1)\rangle_{\text{CFT}^{\otimes m}}\right)^n}\right]. \quad (49)$$

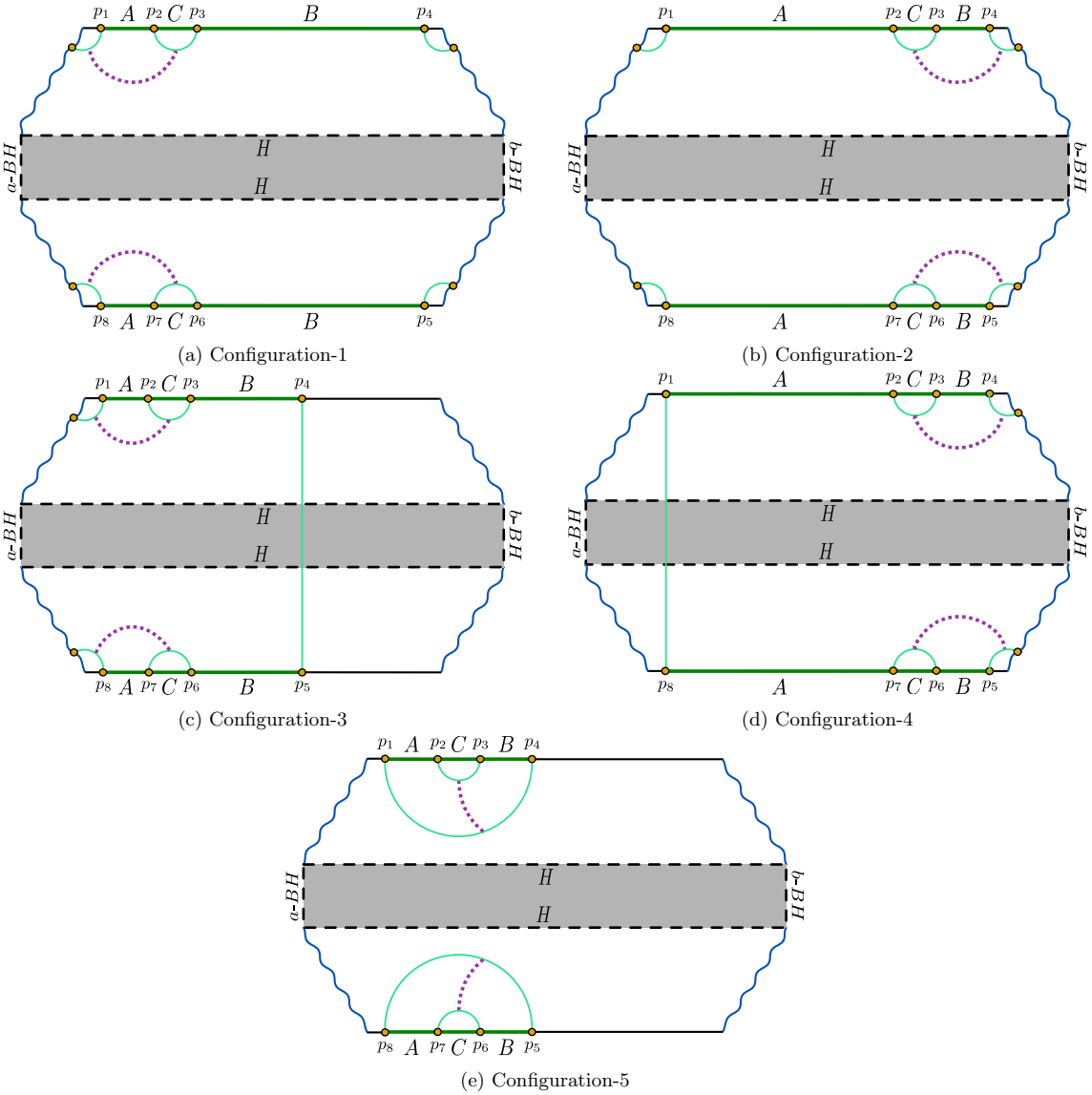

(a) Configuration-1 (b) Configuration-2

(c) Configuration-3 (d) Configuration-4

(e) Configuration-5

Fig. 6 Schematics depicts all the possible contributions to the reflected entropy for the case of two disjoint subsystems A and B where the contraction of the correlator leads to the similar result

Note that the two point function in the above equation cancel from the numerator and denominator in the replica limit. Thus the dominant correlator to the Rényi reflected entropy in this case may be expressed as

$$S^R_{n,m}(A:B) = 2\frac{1}{1-n} \log \frac{\langle \sigma_{g_B^{-1}}(a_1)\sigma_{g_A}(p_1)\sigma_{g_A^{-1}}(p_2)\sigma_{g_B}(p_3)\rangle_{\text{CFT}^{\otimes mn}}}{\langle \sigma_{g_m^{-1}}(a_1)\sigma_{g_m}(p_1)\sigma_{g_m^{-1}}(p_2)\sigma_{g_m}(p_3)\rangle_{\text{CFT}^{\otimes m}}}. \tag{50}$$

Finally, the reflected entropy for the two disjoint subsystems for this configuration may be obtained as follows [31,136]

$$S^R_{\text{eff}}(A:B) = \frac{2c}{3}\log\left(\frac{1+\sqrt{x}}{1-\sqrt{x}}\right),$$

$$x = \frac{\sinh\frac{\pi(p_2-p_1)}{\beta}\sinh\frac{\pi(a_1+p_1)}{\beta}}{\sinh\frac{\pi(p_3-p_1)}{\beta}\sinh\frac{\pi(a_1+p_2)}{\beta}}. \tag{51}$$

Configuration-2

This configuration Fig. 6a is similar to the previous case and the computation of the reflected entropy for the two disjoint subsystems in this case follow the same analysis. However the twist field correlator in Eq. (48) factorizes to the respective contraction in the large central charge limit

$$S^R_{n,m}(A:B) = 2\frac{1}{1-n}\log\left[\frac{\langle\sigma_{g_A^{-1}}(a_1)\sigma_{g_A}(p_1)\rangle_{\text{CFT}^{\otimes mn}}}{\langle\sigma_{g_m^{-1}}(a_1)\sigma_{g_m}(p_1)\rangle_{\text{CFT}^{\otimes m}}}\times\frac{\langle\sigma_{g_A^{-1}}(p_2)\sigma_{g_B}(p_3)\sigma_{g_B^{-1}}(p_4)\sigma_{g_A}(b_1)\rangle_{\text{CFT}^{\otimes mn}}}{\left(\langle\sigma_{g_m^{-1}}(p_2)\sigma_{g_m}(p_3)\sigma_{g_m^{-1}}(p_4)\sigma_{g_m}(b_1)\rangle_{\text{CFT}^{\otimes m}}\right)^n}\right]. \tag{52}$$

From the above equation, the dominant contribution to the reflected entropy arises from the four point twist correlator. Therefore we may obtain the reflected entropy for this configuration as [31,136]

$$S^R_{\text{eff}}(A:B) = \frac{2c}{3}\log\left(\frac{1+\sqrt{x}}{1-\sqrt{x}}\right),$$
$$x = \frac{\sinh\frac{\pi(p_4-p_3)}{\beta}\sinh\frac{\pi(b_1+p_2)}{\beta}}{\sinh\frac{\pi(p_3-p_2)}{\beta}\sinh\frac{\pi(b_1+p_4)}{\beta}}. \tag{53}$$

Configuration- 3 and 4

It may be observed from Fig. 6c that this case is similar to the configuration-3 and the dominant contribution to the reflected entropy is given by Eq. (50). The only difference in this case arises from the two point correlator involving the twist operators located on the points p_4 and p_8 which is obtained after the factorization in the large central charge limit. However this does not contribute to the reflected entropy in the replica limit as it cancels out from the numerator and the denominator as earlier. Hence the reflected entropy in this case is given by Eq. (51).

For the configuration-4 as depicted in Fig. 2d, we follow arguments similar to those described above for the configuration-3 and obtain the reflected entropy from Eq. (53).

Configuration- 5

In this case, the reflected entropy for the two disjoint subsystems may be obtained by utilizing the procedure described in [136]. Since this case involves four point twist correlator as the dominant contribution to the reflected entropy this may be given as

$$S^R_{\text{eff}}(A:B) = \frac{2c}{3}\log\left(\frac{1+\sqrt{x}}{1-\sqrt{x}}\right),$$
$$x = \frac{\sinh\frac{\pi(p_2-p_1)}{\beta}\sinh\frac{\pi(p_4-p_3)}{\beta}}{\sinh\frac{\pi(p_3-p_2)}{\beta}\sinh\frac{\pi(p_4-p_2)}{\beta}}. \tag{54}$$

Configuration-6

In this case, the computation of the reflected entropy involves a nontrivial contribution from the twist operators located at the QES point a_2 on the a-brane and the points p_2 and p_3 in the radiation reservoir as depicted in Fig. 7a. Here the reflected entropy also incorporates an additional contribution from the Weyl factor associated with the QES point a_2. Thus the Rényi reflected entropy in this case may be obtained as

$$S^R_{n,m}(A:B) = 2\frac{1}{1-n}\log\frac{\langle\sigma_{g_B^{-1}g_A}(a_2)\sigma_{g_A^{-1}}(a_1)\sigma_{g_A}(p_1)\sigma_{g_A^{-1}}(p_2)\sigma_{g_B}(p_3)\sigma_{g_B^{-1}}(p_4)\sigma_{g_B}(b_1)\rangle_{\text{CFT}^{\otimes mn}}}{\left(\langle\sigma_{g_m^{-1}}(a_1)\sigma_{g_m}(p_1)\sigma_{g_m^{-1}}(p_2)\sigma_{g_m}(p_3)\sigma_{g_m^{-1}}(p_4)\sigma_{g_m}(b_1)\rangle_{\text{CFT}^{\otimes m}}\right)^n}, \tag{55}$$

where the factor 2 involves the contribution to the reflected entropy from the other copy of the radiation reservoir. In the large central charge limit, the correlator in Eq. (55) factorizes to the following contraction

$$S^R_{n,m}(A:B) = 2\frac{1}{1-n}\log\frac{\left\langle\sigma_{g_A^{-1}}(a_1)\sigma_{g_A}(p_1)\right\rangle\left\langle\sigma_{g_B^{-1}g_A}(a_2)\sigma_{g_A^{-1}}(p_2)\sigma_{g_B}(p_3)\right\rangle\left\langle\sigma_{g_B^{-1}}(p_4)\sigma_{g_B}(b_1)\right\rangle}{\left(\left\langle\sigma_{g_m^{-1}}(a_1)\sigma_{g_m}(p_1)\right\rangle\left\langle\sigma_{g_m^{-1}}(p_2)\sigma_{g_m}(p_3)\right\rangle\left\langle\sigma_{g_m^{-1}}(p_4)\sigma_{g_m}(b_1)\right\rangle\right)^n}. \tag{56}$$

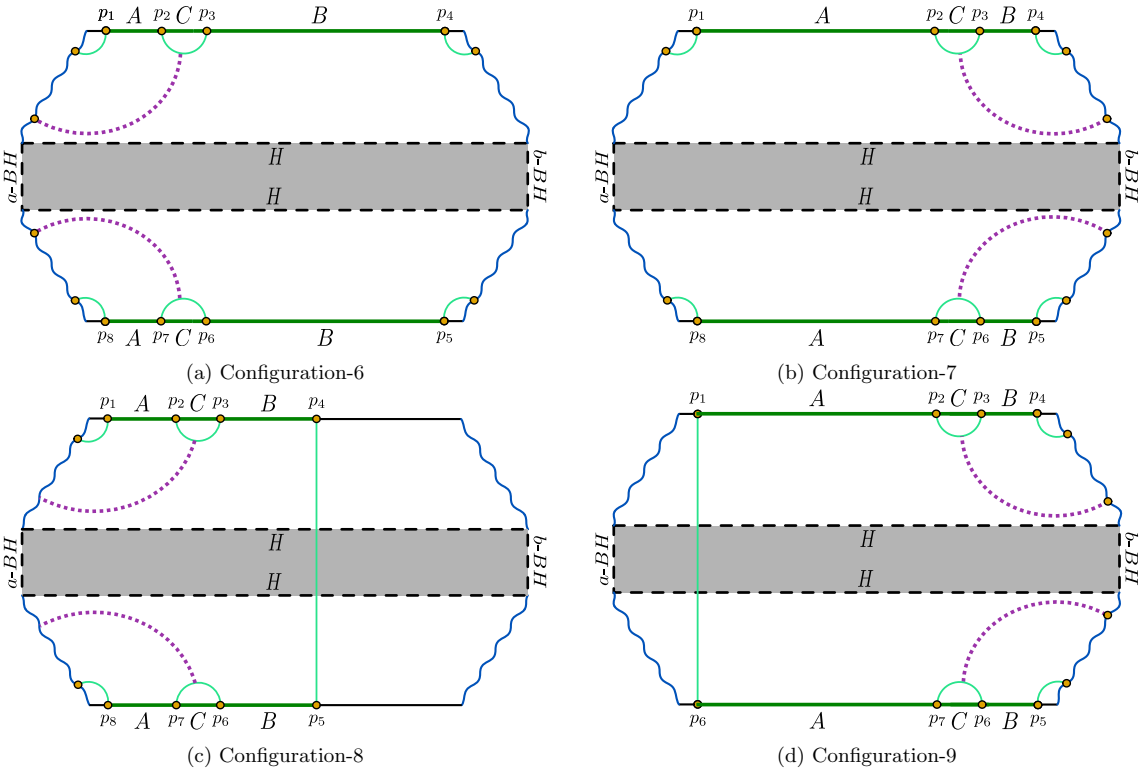

Fig. 7 Schematics depicts all the possible contributions to the reflected entropy for the case of two disjoint subsystems A and B where we get non trivial cross section from the entanglement island

From the above equation, the dominant correlator for this configuration arises from the three point twist correlator while the other contributions to the reflected entropy cancel from the numerator and denominator in the replica limit. Hence the Rényi reflected entropy may be expressed as follows

$$S^R_{n,m}(A:B) = 2\frac{1}{1-n}\log\frac{\langle\sigma_{g_B^{-1}g_A}(a_2)\sigma_{g_A^{-1}}(p_2)\sigma_{g_B}(p_3)\rangle}{\left(\langle\sigma_{g_m^{-1}}(p_2)\sigma_{g_m}(p_3)\rangle\right)^n}. \tag{57}$$

Finally in the replica limit, the reflected entropy of the two disjoint subsystems for this case may be given by

$$S^R_{\text{eff}}(A:B) = \frac{2c}{3}\log\left[\frac{\beta\left(\cosh\left(\frac{2\pi(R-a_2)}{\beta}\right)-1\right)}{\pi r\sinh\left(\frac{2\pi a_2}{\beta}\right)}\right], \tag{58}$$

where R and r are related to the points p_2 and p_3 as $R = (p_3+p_2)/2$ and $r = (p_3-p_2)/2$. Now we may obtain the generalized reflected entropy using the island formula described in Eq. (13) as

$$S^R_{\text{gen}}(A:B) = 2\Phi_0 + \frac{4\pi\Phi_r}{\beta}\coth\left(\frac{2\pi a_2}{\beta}\right) + \frac{2c}{3}\log\left[\frac{\beta\left(\cosh\left(\frac{2\pi(R-a_2)}{\beta}\right)-1\right)}{\pi r\sinh\left(\frac{2\pi a_2}{\beta}\right)}\right]. \tag{59}$$

Configuration-7

This configuration is similar to the previous case however the dominant correlator for the reflected entropy for the two disjoint subsystems now involves a QES point b_2 located on the b-brane as shown in Fig. 7b. Thus the factorization of the twist correlator for the Rényi reflected entropy in the large central charge limit may be given by

$$S^R_{n,m}(A:B) = 2\frac{1}{1-n}\log\frac{\left\langle\sigma_{g_A^{-1}}(a_1)\sigma_{g_A}(p_1)\right\rangle\left\langle\sigma_{g_B^{-1}g_A}(b_2)\sigma_{g_A^{-1}}(p_2)\sigma_{g_B}(p_3)\right\rangle\left\langle\sigma_{g_B^{-1}}(p_4)\sigma_{g_B}(b_1)\right\rangle}{\left(\left\langle\sigma_{g_m^{-1}}(a_1)\sigma_{g_m}(p_1)\right\rangle\left\langle\sigma_{g_m^{-1}}(p_2)\sigma_{g_m}(p_3)\right\rangle\left\langle\sigma_{g_m^{-1}}(p_4)\sigma_{g_m}(b_1)\right\rangle\right)^n}. \tag{60}$$

Note that the dominant correlator from the above equation arises from the three point twist correlator involving the points p_2, p_3 and b_2 while the other contributions to the reflected entropy cancel from the numerator and denominator in the replica limit. Hence the Rényi reflected entropy may be obtained as follows

$$S^R_{n,m}(A:B) = 2\frac{1}{1-n}\log\frac{\langle\sigma_{g_B^{-1}g_A}(b_2)\sigma_{g_A^{-1}}(p_2)\sigma_{g_B}(p_3)\rangle}{\left(\langle\sigma_{g_m^{-1}}(p_2)\sigma_{g_m}(p_3)\rangle\right)^n}. \tag{61}$$

Finally in the replica limit the expression for the reflected entropy in this case is given by the following

$$S^R_{\text{eff}}(A:B) = \frac{2c}{3}\log\left[\frac{\beta\left(\cosh\left(\frac{2\pi(R-b_2)}{\beta}\right)-1\right)}{\pi r\sinh\left(\frac{2\pi b_2}{\beta}\right)}\right], \tag{62}$$

where R and r are related to the points p_2 and p_3 as $R = (p_3+p_2)/2$ and $r = (p_3-p_2)/2$. Once again we may obtain the generalized reflected entropy using the island formula in Eq. (13) as follow

$$S^R_{\text{gen}}(A:B) = 2\Phi_0 + \frac{4\pi\Phi_r}{\beta}\coth\left(\frac{2\pi b_2}{\beta}\right) + \frac{2c}{3}\log\left[\frac{\beta\left(\cosh\left(\frac{2\pi(R-b_2)}{\beta}\right)-1\right)}{\pi r\sinh\left(\frac{2\pi b_2}{\beta}\right)}\right]. \tag{63}$$

Configuration-8 and 9

In these configurations, the computation of the reflected entropy follows a similar analysis to that described in configuration-3 and 4. The dominant twist correlators in these cases are given by the Eqs. (57) and (61) in the large central charge limit. The only difference in configuration-8 as depicted in Fig. 7c arises from the two point correlator involving the twist operators located at the points p_4 and p_8 however this contribution to the reflected entropy cancel from the numerator and denominator in the replica limit. Hence the expression for the reflected entropy in the above configuration is given by Eq. (59) in the replica limit.

For the configuration-9 (Fig. 7d), we may employ similar arguments as described for the configuration-8 to compute the reflected entropy of two disjoint subsystems. Thus the reflected entropy in this case is given by Eq. (63) in the replica limit.

Configuration-10

The reflected entropy in this configuration involves twist operators located on both the radiation reservoirs and the a and b-branes as depicted in Fig. 8a. The Rényi reflected entropy in this case may be obtained as

$$S^R_{n,m}(A:B) = \frac{1}{1-n}\log\left[\frac{\left\langle\sigma_{g_A^{-1}}(a_1)\sigma_{g_A}(p_1)\sigma_{g_A^{-1}}(p_2)\sigma_{g_B}(p_3)\sigma_{g_B^{-1}}(p_4)\sigma_{g_B}(b_1)\right\rangle}{\left\langle\sigma_{g_m^{-1}}(a_1)\sigma_{g_m}(p_1)\sigma_{g_m^{-1}}(p_2)\sigma_{g_m}(p_3)\sigma_{g_m^{-1}}(p_4)\sigma_{g_m}(b_1)\right\rangle}\frac{\left\langle\sigma_{g_A}(a_2)\sigma_{g_A^{-1}}(p_5)\sigma_{g_A}(p_6)\sigma_{g_B^{-1}}(p_7)\sigma_{g_B}(p_8)\sigma_{g_B^{-1}}(b_2)\right\rangle_{\text{CFT}^{\otimes mn}}}{\left\langle\sigma_{g_m}(a_2)\sigma_{g_m^{-1}}(p_5)\sigma_{g_m}(p_6)\sigma_{g_m^{-1}}(p_7)\sigma_{g_m}(p_8)\sigma_{g_m^{-1}}(b_2)\right\rangle^n_{\text{CFT}^{\otimes m}}}\right]. \tag{64}$$

The factorization of the above correlator to the respective contraction in the large central charge limit is given by the following equation

$$S^R_{n,m}(A:B) = \frac{1}{1-n}\log\left[\frac{\left\langle\sigma_{g_A^{-1}}(a_1)\sigma_{g_A}(p_1)\right\rangle\left\langle\sigma_{g_A^{-1}}(p_2)\sigma_{g_B}(p_3)\sigma_{g_A}(p_6)\sigma_{g_B^{-1}}(p_7)\right\rangle}{\left(\left\langle\sigma_{g_m^{-1}}(a_1)\sigma_{g_m}(p_1)\right\rangle\left\langle\sigma_{g_m^{-1}}(p_2)\sigma_{g_m}(p_3)\sigma_{g_m}(p_6)\sigma_{g_m^{-1}}(p_7)\right\rangle\right)^n}\frac{\left\langle\sigma_{g_B^{-1}}(p_4)\sigma_{g_B}(b_1)\right\rangle\left\langle\sigma_{g_A}(a_2)\sigma_{g_A^{-1}}(p_5)\right\rangle\left\langle\sigma_{g_B}(p_8)\sigma_{g_B^{-1}}(b_2)\right\rangle}{\left(\left\langle\sigma_{g_m^{-1}}(p_4)\sigma_{g_m}(b_1)\right\rangle\left\langle\sigma_{g_m}(a_2)\sigma_{g_m^{-1}}(p_5)\right\rangle\left\langle\sigma_{g_m}(p_8)\sigma_{g_m^{-1}}(b_2)\right\rangle\right)^n}\right], \tag{65}$$

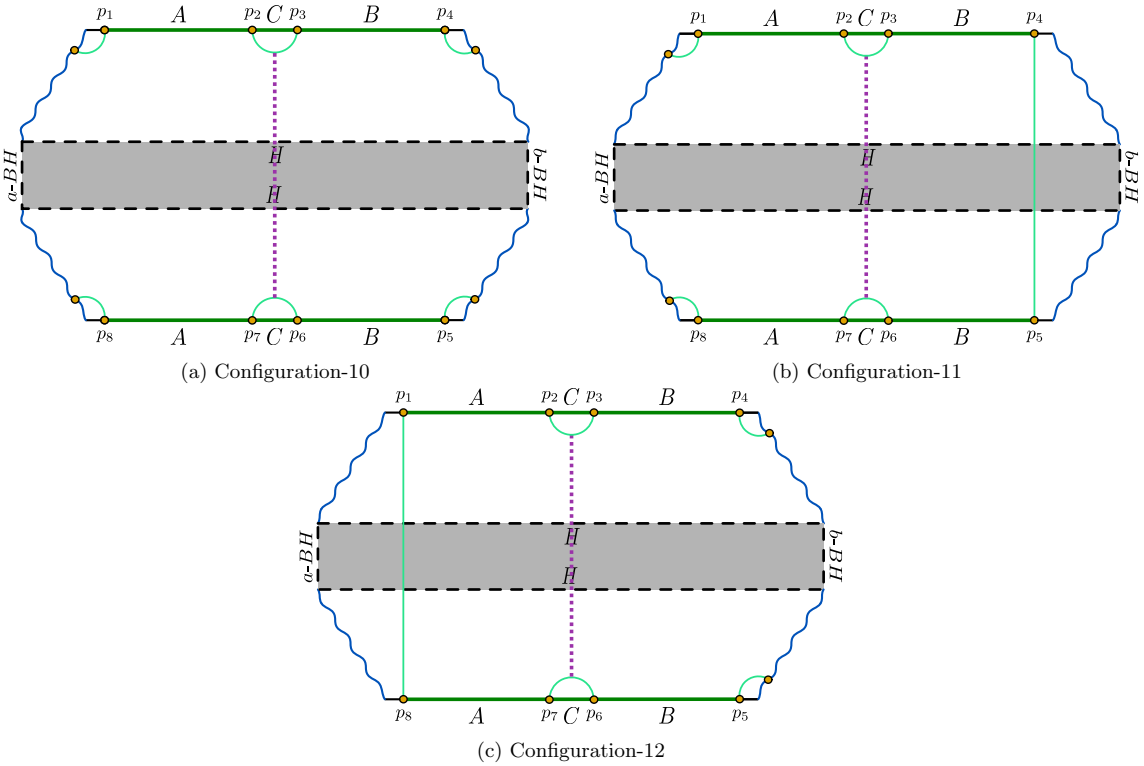

(a) Configuration-10 (b) Configuration-11

(c) Configuration-12

Fig. 8 The corresponding diagrams depict non-trivial cross section extending between the TFD copies of the radiation reservoirs

where the Weyl factors associated with the points on the branes cancel from the numerator and denominator in the replica limit. The dominant twist correlator in this case for the reflected entropy involves the four point correlator with the twist operators located on both the radiation reservoirs. Hence the Rényi reflected entropy is given by

$$S^R_{n,m}(A:B) = \frac{1}{1-n} \times \log \frac{\left\langle \sigma_{g_A^{-1}}(p_2)\sigma_{g_B}(p_3)\sigma_{g_A}(p_6)\sigma_{g_B^{-1}}(p_7)\right\rangle}{\left(\left\langle \sigma_{g_m^{-1}}(p_2)\sigma_{g_m}(p_3)\sigma_{g_m}(p_6)\sigma_{g_m^{-1}}(p_7)\right\rangle\right)^n}, \tag{66}$$

where the other two point twist correlators in the above equation cancel from the numerator and denominator in the replica limit. Finally, the reflected entropy for this case in the replica limit may be obtained as follows

$$S^R_{\text{eff}}(A:B) = \frac{2c}{3}\log\left[\frac{\beta\cosh\left(\frac{2\pi t}{\beta}\right)}{\pi r}\right]. \tag{67}$$

In Eq. (67), r is related to the points p_2 and p_3 as $r = (p_3 - p_2)/2$.

Configuration-11 and 12

In these configurations (Fig. 8b, c), the computation of the reflected entropy follows similar analysis as described in the configuration-10. The only difference in these cases arise from the two point correlators with the twist operators located at the points p_4 and p_8 in the radiation reservoirs for the first while the other configuration-12 (Fig. 8c) incorporates the twist operators located at the points p_1 and p_5. However these contributions to the reflected entropy for these cases cancel from the numerator and denominator in the replica limit. Thus the expression of the reflected entropies in these configurations are given by Eq. (67).

Configuration-13

In this case, the reflected entropy for the two disjoint subsystems A and B involves the twist operators located on both the radiation reservoirs as depicted in Fig. 9a. The Rényi reflected entropy in this scenario may be expressed as follows

$$S^R_{n,m}(A:B)=\frac{1}{1-n}\log\left[\frac{\left\langle\sigma_{g_A^{-1}}(a_1)\sigma_{g_A}(p_1)\sigma_{g_A^{-1}}(p_2)\sigma_{g_B}(p_3)\sigma_{g_B^{-1}}(p_4)\right.}{\left(\left\langle\sigma_{g_m^{-1}}(a_1)\sigma_{g_m}(p_1)\sigma_{g_m^{-1}}(p_2)\sigma_{g_m}(p_3)\sigma_{g_m^{-1}}(p_4)\right.\right.}\frac{\sigma_{g_A}(a_2)\sigma_{g_A^{-1}}(p_5)\sigma_{g_A}(p_6)\sigma_{g_B^{-1}}(p_7)\sigma_{g_B}(p_8)\Big\rangle_{\mathrm{CFT}^{\otimes mn}}}{\left.\left.\sigma_{g_m}(a_2)\sigma_{g_m^{-1}}(p_5)\sigma_{g_m}(p_6)\sigma_{g_m^{-1}}(p_7)\sigma_{g_m}(p_8)\Big\rangle_{\mathrm{CFT}^{\otimes m}}\right)^n}\right]. \tag{68}$$

In the large central charge limit, the correlator in Eq. (68) factorizes to the respective contraction as follows

$$S^R_{n,m}(A:B)=\frac{1}{1-n}\log\left[\frac{\left\langle\sigma_{g_A^{-1}}(p_2)\sigma_{g_B}(p_3)\sigma_{g_B^{-1}}(p_4)\sigma_{g_A}(p_6)\sigma_{g_B^{-1}}(p_7)\sigma_{g_B}(p_8)\right\rangle}{\left(\left\langle\sigma_{g_m^{-1}}(p_2)\sigma_{g_m}(p_3)\sigma_{g_m^{-1}}(p_4)\sigma_{g_m}(p_6)\sigma_{g_m^{-1}}(p_7)\sigma_{g_m}(p_8)\right\rangle\right)^n}\frac{\left\langle\sigma_{g_A^{-1}}(a_1)\sigma_{g_A}(p_1)\right\rangle\left\langle\sigma_{g_A^{-1}}(a_2)\sigma_{g_A}(p_5)\right\rangle}{\left(\left\langle\sigma_{g_m^{-1}}(a_1)\sigma_{g_m}(p_1)\right\rangle\left\langle\sigma_{g_m^{-1}}(a_2)\sigma_{g_m}(p_5)\right\rangle\right)^n}\right]. \tag{69}$$

The dominant twist correlator in this case for the reflected entropy involves the six point function with the twist operators located on both the radiation reservoirs, however the other two point twist correlators in Eq. (69) cancel from the numerator and denominator in the replica limit. Hence the Rényi reflected entropy is given as

$$S^R_{n,m}(A:B)=\frac{1}{1-n}\log\frac{\left\langle\sigma_{g_A^{-1}}(p_2)\sigma_{g_B}(p_3)\sigma_{g_B^{-1}}(p_4)\sigma_{g_A}(p_6)\sigma_{g_B^{-1}}(p_7)\sigma_{g_B}(p_8)\right\rangle}{\left(\left\langle\sigma_{g_m^{-1}}(p_2)\sigma_{g_m}(p_3)\sigma_{g_m^{-1}}(p_4)\sigma_{g_m}(p_6)\sigma_{g_m^{-1}}(p_7)\sigma_{g_m}(p_8)\right\rangle\right)^n}. \tag{70}$$

We utilize a technique termed as inverse doubling trick to compute the above dominant correlator [175]. In this context, the six point function in the CFT_2 reduces to a three point function in the $BCFT_2$ and the expression for the reflected entropy may be obtained in the appropriate OPE channel by following a similar analysis to that described in [175]

$$S^R_{\mathrm{eff}}(A:B)=\frac{c}{3}\log\left[\frac{\mathrm{sech}(\frac{2\pi t}{\beta})\sqrt{r^2+(R-r_2)^2}\sqrt{r^2+R^2+2Rr_2\cosh(\frac{4\pi t}{\beta})+r_2^2}}{r_2 r}\right], \tag{71}$$

where R and r are related to the points p_2 and p_3 as $R=(p_3+p_2)/2$ and $r=(p_3-p_2)/2$.

Configuration-14

This configuration is similar to above case and the twist correlator for the Rényi reflected entropy factorizes to the respective contraction in the large central charge limit as follows

$$S^R_{n,m}(A:B)=\frac{1}{1-n}\log\left[\frac{\left\langle\sigma_{g_A}(p_1)\sigma_{g_A^{-1}}(p_2)\sigma_{g_B}(p_3)\sigma_{g_A^{-1}}(p_5)\sigma_{g_B}(p_6)\sigma_{g_B^{-1}}(p_7)\right\rangle}{\left(\left\langle\sigma_{g_m}(p_1)\sigma_{g_m^{-1}}(p_2)\sigma_{g_m}(p_3)\sigma_{g_m^{-1}}(p_5)\sigma_{g_m}(p_6)\sigma_{g_m^{-1}}(p_7)\right\rangle\right)^n}\frac{\left\langle\sigma_{g_B}(b_1)\sigma_{g_B^{-1}}(p_4)\right\rangle\left\langle\sigma_{g_B^{-1}}(b_2)\sigma_{g_B}(p_8)\right\rangle}{\left(\left\langle\sigma_{g_m^{-1}}(b_1)\sigma_{g_m}(p_3)\right\rangle\left\langle\sigma_{g_m^{-1}}(b_2)\sigma_{g_m}(p_8)\right\rangle\right)^n}\right]. \tag{72}$$

In this case, the dominant correlator in the above equation involves a six point twist correlator, however the other two point twist correlators cancel from the numerator and the denominator. Thus the Rényi reflected entropy may be obtained as

$$S^R_{n,m}(A:B)=\frac{1}{1-n}\log\frac{\left\langle\sigma_{g_A}(p_1)\sigma_{g_A^{-1}}(p_2)\sigma_{g_B}(p_3)\sigma_{g_A^{-1}}(p_5)\sigma_{g_B}(p_6)\sigma_{g_B^{-1}}(p_7)\right\rangle}{\left(\left\langle\sigma_{g_m}(p_1)\sigma_{g_m^{-1}}(p_2)\sigma_{g_m}(p_3)\sigma_{g_m^{-1}}(p_5)\sigma_{g_m}(p_6)\sigma_{g_m^{-1}}(p_7)\right\rangle\right)^n}. \tag{73}$$

On utilization of the techniques discussed in [175], the reflected entropy for the two disjoint subsystems is given by the following equation

$$S^R_{\mathrm{eff}}(A:B)=\frac{c}{3}\log\left[\frac{\mathrm{sech}(\frac{2\pi t}{\beta})\sqrt{r^2+(R-r_2)^2}\sqrt{r^2+R^2+2Rr_2\cosh(\frac{4\pi t}{\beta})+r_2^2}}{r_2 r}\right], \tag{74}$$

where R and r are related to the points p_2 and p_3 as $R=(p_3+p_2)/2$ and $r=(p_3-p_2)/2$.

Configuration-15 and 16

In these configurations, the computation of the reflected entropies for the two disjoint subsystems A and B follow a similar analysis as described for the configurations-13 and

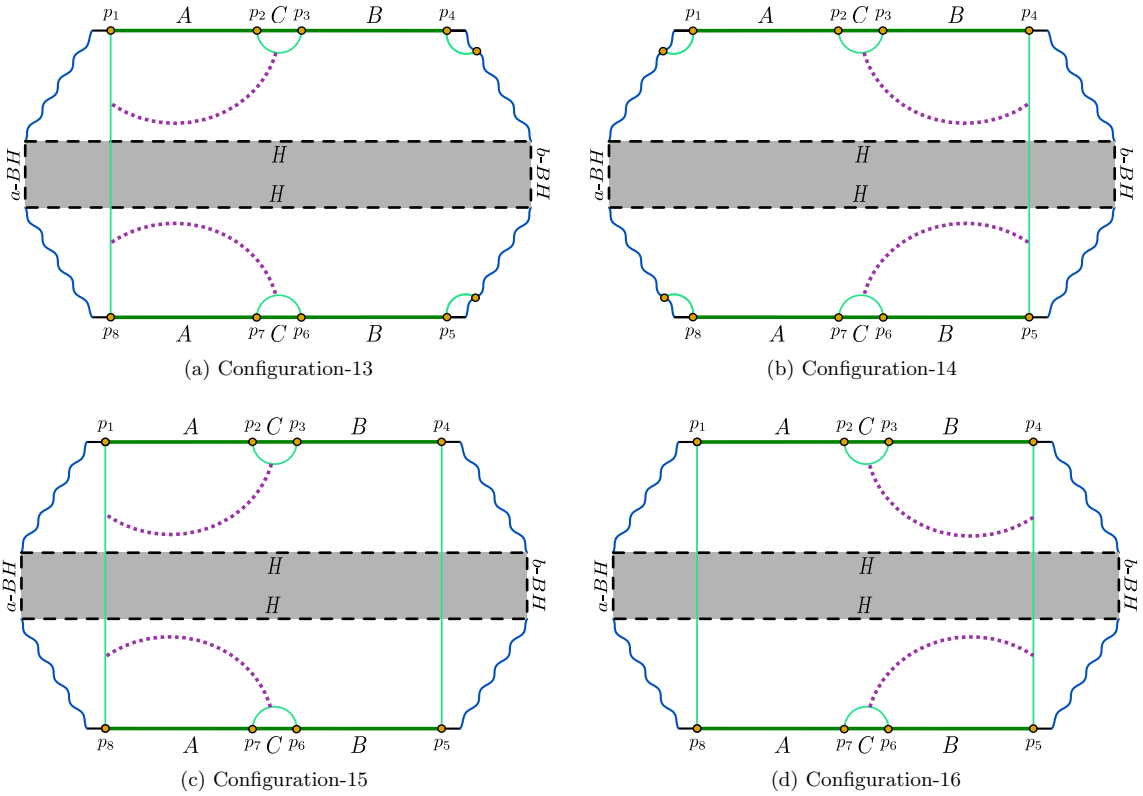

(a) Configuration-13 (b) Configuration-14

(c) Configuration-15 (d) Configuration-16

Fig. 9 Starting two figures indicate connected phase of the entanglement island with non-trivial cross section however later diagrams depict disconnected phase of the entanglement island with cross section ending the Hartman–Maldacena surface

14. Here the dominant correlators for these configurations are given by the Eqs. (70) and (73). The only difference in these cases arise from the two point correlators with the twist operators located at the points p_4 and p_8 for the first (Fig. 9c) while the other configuration-16 (Fig. 9d) incorporates the twist operators located at the points p_1 and p_5 in the radiation reservoirs. However these contributions to the reflected entropy for these cases cancel from the numerator and denominator in the replica limit. Finally, the reflected entropy for these configurations are given by the Eqs. (71) and (74).

3.2 Entanglement wedge cross section

In this subsection, we compute the bulk EWCS for the various mixed states described by the two adjacent and disjoint subsystems located in both the radiation reservoirs for which the field theory computations were described in the earlier sections. In this context, we observed a rich phase structure for the EWCS arising from the various contributions from different relative sizes of the two adjacent and disjoint subsystems as depicted in the Figs. 2, 3, 4, 5, 6, 7, 8 and 9. In particular, we utilized the embedding space formalism to compute the bulk EWCS for different configurations.

3.2.1 Adjacent subsystems

We first consider the two adjacent subsystems A and B in both the copies of the radiation reservoirs and compute the EWCS for all the possible contributions while considering different sizes of the subsystems.

Configuration-1

The EWCS for this configuration is shown in Fig. 2a as a dotted line and this may be computed using the result obtained in [147] in the adjacent limit as follows

$$E_W = \frac{c}{3}\log(4z)\,, \qquad z = \frac{\sinh\frac{\pi z_{12}}{\beta}\sinh\frac{\pi z_{34}}{\beta}}{\sinh\frac{\pi z_{23}}{\beta}\sinh\frac{\pi z_{14}}{\beta}}, \tag{75}$$

where z is the cross-ratio at a finite temperature and we have utilized the Brown–Henneaux formula $c = \frac{3}{2G_N}$ [176]. The above result may be expressed in terms of the boundary coordinates of the corresponding subsystems shown in Fig. 2a as follows

$$E_W = \frac{c}{3}\log\left[4\frac{\sinh\frac{\pi(p_2-p_1)}{\beta}\sinh\frac{\pi(a_1+p_2)}{\beta}}{\sinh\frac{\pi(a_1+p_1)}{\beta}\sinh\frac{\pi(\epsilon)}{\beta}}\right]. \tag{76}$$

Interestingly the field theory replica technique result for the the reflected entropy described in Eq. (23) matches exactly with twice the bulk EWCS in Eq. (75) for the two adjacent subsystems in accordance with the proposed holographic duality in [31,136].

Configuration-2

As depicted in Fig. 2b, the bulk EWCS for this configuration may be obtained by following a similar analysis as discussed in the previous configuration. Hence the expression for the EWCS is given by

$$E_W = \frac{c}{3}\log\left[4\frac{\sinh\frac{\pi(p_3-p_2)}{\beta}\sinh\frac{\pi(b_1+p_2)}{\beta}}{\sinh\frac{\pi(b_1+p_3)}{\beta}\sinh\frac{\pi(\epsilon)}{\beta}}\right], \tag{77}$$

where ϵ is the UV cutoff. Once again the replica technique result in Eq. (26) matches with twice the bulk EWCS in Eq. (77) in agreement with the proposed holographic duality in [31,136].

Configuration-3 and 4

The configuration-3 is similar to the case-1. However the only difference in this configuration arises from the entanglement wedge of the subsystem $A \cup B$ as described in Fig. 2c. Thus the bulk EWCS for the configuration-3 may be obtained from Eq. (76).

On utilization of similar argument for the configuration-4 which is analogous to case-2 as shown in Fig. 2d. Therefore, the bulk EWCS for the configuration-4 is given by Eq. (77).

Configuration-5

The computation of the bulk EWCS for this configuration as shown in Fig. 2e is trivial since it reduces to the usual expression of the EWCS in the context of the AdS/CFT scenario. Therefore the bulk EWCS is given by

$$E_W = \frac{c}{3}\log\left[4\frac{\sinh\frac{\pi(p_3-p_2)}{\beta}\sinh\frac{\pi(p_3-p_2)}{\beta}}{\sinh\frac{\pi(p_3-p_1)}{\beta}\sinh\frac{\pi(\epsilon)}{\beta}}\right]. \tag{78}$$

Once again twice of the above bulk EWCS exactly matches with the replica technique results in Eq. (27) which is consistent with the holographic duality described in [31,136].

Configuration-6

The bulk EWCS in this configuration involves QES point located on the a-brane and the point p_2 situated in the radiation reservoir as shown in the Fig. 3a. To compute the bulk EWCS for this configuration, we utilize the embedding space formalism which involves following coordinate transformations [51,91]

$$\begin{aligned}
T_1(z,t) &= z_h\sqrt{\frac{1}{z^2}-\frac{1}{z_h^2}}\cosh\left(\frac{t}{z_h}\right),\\
T_2(z,t) &= \frac{z_h\sinh\left(\frac{x}{z_h}\right)}{z},\\
X_1(z,t) &= z_h\sqrt{\frac{1}{z^2}-\frac{1}{z_h^2}}\sinh\left(\frac{t}{z_h}\right),\\
X_2(z,t) &= \frac{z_h\cosh\left(\frac{x}{z_h}\right)}{z}.
\end{aligned} \tag{79}$$

where z_h is related to the inverse temperature as $z_h = \frac{\beta}{2\pi}$. Note that, the AdS_3 BTZ black hole metric may be reduced to the embedding metric using the above coordinate transformations as follows [51,91]

$$ds^2 = dX_1^2 + dX_2^2 - dT_1^2 - dT_2^2\,. \tag{80}$$

In the above background, the expression of the geodesic length connecting two arbitrary points is given by

$$L = \cosh^{-1}\left(X_1X_1' + X_2X_2' - T_1T_1' - T_2T_2'\right), \tag{81}$$

where the unprimed and the primed coordinates are the location of the arbitrary points in term of the embedding coordinates. For this configuration, the endpoints of the bulk EWCS in the BTZ coordinates are defined as (p_2, ϵ, t) and $(a_2, z_{\rm QES}, t)$. Finally, we may obtain the bulk EWCS utilizing the Eqs. (81) and (79) as

$$E_W = \frac{c}{3}\cosh^{-1}\left[\frac{z_h^2\left(\cosh\left(\frac{a_2-p_2}{z_h}\right)-1\right)}{z_{\rm QES}\epsilon}\right], \tag{82}$$

where $z_{\rm QES}$ may be obtained using the profile of the a-brane as $z_{\rm QES}\,k = z_h\sinh\left(\frac{a_2}{z_h}\right)$ with constant $k = 1$ [51]. Hence, the expression of the bulk EWCS becomes

$$E_W = \frac{c}{3}\log\left[\frac{\beta}{\pi}\frac{\cosh\left(\frac{2\pi(a_2-p_2)}{\beta}\right)-1}{\sinh\left(\frac{2\pi a_2}{\beta}\right)}\right], \tag{83}$$

where we have removed divergent term. In the above equation, we have utilized a relation between inverse temperature and z_h as $z_h = \frac{\beta}{2\pi}$. Once again twice of the above bulk EWCS exactly matches with the replica technique result in Eq. (31) which is consistent with the proposed holographic duality in [31,136].

Configuration-7

For this configuration, the computation of the bulk EWCS follows a similar analysis as described in the previous case. However the bulk EWCS for this configuration involves a point b_2 located at the b-brane. Hence the expression of the bulk EWCS is given as

$$E_W = \frac{c}{3}\log\left[\frac{\beta}{\pi}\frac{\cosh\left(\frac{2\pi(b_2-p_2)}{\beta}\right)-1}{\sinh\left(\frac{2\pi b_2}{\beta}\right)}\right]. \tag{84}$$

Once again the replica technique result in Eq. (35) exactly matches with twice of the above bulk EWCS in accordance with the proposed holographic duality.

Configuration-8 and 9

For these configurations, the computation of the bulk EWCS follows a similar analysis described in the configurations 6 and 7. However the enclosed entanglement wedge regions for the subsystem $A\cup B$ in these two configurations are different as shown in the Fig. 3c and d. Thus the expressions of the bulk EWCS for the configurations 8 and 9 are given by the Eqs. (83) and (84) respectively.

Configuration-10

The computation of the bulk EWCS for this configuration involves the endpoints (p_2,ϵ,t) and $(p_2,\epsilon,-t+i\beta/2)$ which are located in both the radiation reservoirs as depicted in Fig. 4a. Utilizing the Eqs. (81) and (79), we may obtain the expression of the bulk EWCS as follows

$$E_W = \frac{c}{3}\log\left[\frac{\beta}{\pi}\cosh\left(\frac{2\pi t}{\beta}\right)\right], \tag{85}$$

where we have removed divergent term. Note that twice of above the bulk EWCS exactly matches with the replica technique result for the reflected entropy described in Eq. (40) which is consistent with the holographic duality in [31,136].

Configuration-11 and 12

The computation of the bulk EWCS for these configurations follow a similar analysis described in the configuration-10. The only difference in these configurations arises from the enclosed entanglement wedge regions for the subsystem $A\cup B$ as shown in the Fig. 4b and c. Thus the expressions of the bulk EWCS for the configurations 11 and 12 are given by Eq. (85).

Configuration-13

For the computation of the bulk EWCS in this configuration, we may utilize a coordinate transformation which relates the AdS_3 BTZ metric described in Eq. (6) to Poincare metric as follows[8]

$$\begin{aligned} T &= \sqrt{1-\frac{z^2}{z_h^2}}e^{\frac{x}{z_h}}\sinh\left(\frac{t}{z_h}\right)\\ X &= \sqrt{1-\frac{z^2}{z_h^2}}e^{\frac{x}{z_h}}\cosh\left(\frac{t}{z_h}\right)\\ Z &= \frac{ze^{\frac{x}{z_h}}}{z_h}, \end{aligned} \tag{86}$$

where T, X, Z are the Poincare coordinates. The bulk EWCS may then be obtained from the following geodesic length formula

$$L = \cosh^{-1}\left[\frac{(X_2-X_1)^2-(T_2-T_1)^2+Z_1^2+Z_2^2}{2Z_1Z_2}\right]. \tag{87}$$

As described in Fig. 5a, the endpoints of the bulk EWCS for this case are given by $\left(r_1\cosh\frac{2\pi t}{\beta}, r_1\sinh\frac{2\pi t}{\beta},\epsilon\right)$ and $\left(x_2, r_2\sinh\frac{2\pi t}{\beta}, z_2\right)$. Note that the bulk EWCS for this configuration describes the following geodesic equation $z_2 = \sqrt{r_2^2(\cosh\frac{2\pi t}{\beta})^2 - x_2^2}$, which is also similar to the Hartman–Maldacena surface discussed in [174]. Thus the expression of the bulk EWCS may be obtained as

$$E_W = \frac{c}{3}\log\left[\frac{(r_1-r_2)\,\mathrm{sech}\left(\frac{2\pi t}{\beta}\right)\sqrt{r_1^2+2r_1r_2\cosh\left(\frac{4\pi t}{\beta}\right)+r_2^2}}{r_1\epsilon}\right], \tag{88}$$

where we have utilized the relation between inverse temperature and z_h. Once again the replica technique result in Eq. (44) exactly matches with twice the bulk EWCS which is consistent with the proposed holographic duality described in [31,136].

Configuration-14

The computation of the bulk EWCS for this configuration follows a similar analysis described in the previous case.

[8] This kind of bulk EWCS was also studied in the article [175] in a different toy model of the brane world geometry.

Thus, the expression of the bulk EWCS may be obtained using Eq. (87) as

$$E_W = \frac{c}{3} \log\left[\frac{(r_1 - r_2)\,\text{sech}\left(\frac{2\pi t}{\beta}\right)\sqrt{r_1^2 + 2r_1 r_2 \cosh\left(\frac{4\pi t}{\beta}\right) + r_2^2}}{r_1 \epsilon}\right]. \tag{89}$$

Interestingly the the replica technique result for the reflected entropy in Eq. (47) exactly matches with twice the above bulk EWCS in accordance with holographic duality.

Configuration-15 and 16

The computation of the bulk EWCS for these configurations as show in Fig. 5c and d follow a similar analysis described in the configuration 13. Hence the expressions of the bulk EWCS for the configurations 15 and 16 are given by the Eqs. (88) and (89) respectively.

3.2.2 Disjoint subsystems

In this subsection, we discuss the computation of the bulk EWCS for the case of two disjoint subsystems A and B which are sandwiched with an auxiliary subsystem C. These subsystems are located in both the copies of the radiation reservoirs described by CFT_2s. In this context, we obtain different possible contributions to the bulk EWCS as depicted in Figs. 6, 7, 8 and 9 with different sizes of the subsystems.

Configuration-1

To compute the bulk EWCS for this configuration, we utilize the result of the bulk EWCS obtained in [147] for two disjoint subsystems A and B at finite temperature in the context of AdS_3/CFT_2 scenario. The corresponding expression of the EWCS may be obtained in terms of the finite temperature cross ratio z as follows

$$E_W = \frac{c}{6}\log\left[1 + 2z + 2\sqrt{z(z+1)}\right], \quad z = \frac{\sinh\frac{\pi z_{12}}{\beta}\sinh\frac{\pi z_{34}}{\beta}}{\sinh\frac{\pi z_{23}}{\beta}\sinh\frac{\pi z_{14}}{\beta}}, \tag{90}$$

where we have used Brown–Henneaux formula $c = 3/2G_N$ [176]. For the configuration described in Fig. 6a, the bulk EWCS may be obtained using the coordinate of the boundary subsystems $A = [p_1, p_2]$ and $B = [p_3, a_1]$ as

$$E_W = 2\frac{c}{6}\log\left[1 + 2z + 2\sqrt{z(z+1)}\right], \quad z = \frac{\sinh\frac{\pi(p_2-p_1)}{\beta}\sinh\frac{\pi(a_1-p_1)}{\beta}}{\sinh\frac{\pi(p_3-p_2)}{\beta}\sinh\frac{\pi(a_1-p_1)}{\beta}}. \tag{91}$$

The above bulk EWCS is consistent with the replica technique result of the reflected entropy in Eq. (51) in accordance with the holographic duality as described in [31,136].

Configuration-2

From the Fig. 6b, we can observe that the bulk EWCS in this configuration may be obtained using a similar analysis followed in the configuration-1. Hence the expression of the bulk EWCS is given by

$$E_W = 2\frac{c}{6}\log\left[1 + 2z + 2\sqrt{z(z+1)}\right], \quad z = \frac{\sinh\frac{\pi(p_4-p_3)}{\beta}\sinh\frac{\pi(b_1+p_2)}{\beta}}{\sinh\frac{\pi(p_4-p_2)}{\beta}\sinh\frac{\pi(b_1+p_2)}{\beta}}. \tag{92}$$

Once again the replica technique result in Eq. (53) exactly matches with twice the bulk EWCS which is consistent with the proposed holographic duality described in [31,136].

Configuration-3 and 4

The computation of the bulk EWCS for these configurations are similar to the cases discussed earlier. However the only difference in these configurations arises from the enclosed entanglement wedge regions for the subsystem $A \cup B$ as shown in Fig. 6c and d. Thus the expression of the bulk EWCS in the configurations 3 and 4 are given by the Eqs. (91) and (92) respectively.

Configuration-5

The computation of the EWCS follows a similar analysis described in [147] in the context of the AdS/CFT scenario. At a finite temperature, the expression of the EWCS in this configuration may be given by the following equation

$$E_W = 2\frac{c}{6}\log\left[1 + 2z + 2\sqrt{z(z+1)}\right], \quad z = \frac{\sinh\frac{\pi(p_2-p_1)}{\beta}\sinh\frac{\pi(p_4-p_3)}{\beta}}{\sinh\frac{\pi(p_3-p_1)}{\beta}\sinh\frac{\pi(p_4-p_1)}{\beta}}. \tag{93}$$

Once again twice of the above bulk EWCS is consistent with the replica technique expression in Eq. (54) in accordance with the proposed holographic duality.

Configuration-6

In this configuration, we follow a similar analysis described in the configuration-6 of the adjacent subsystems to obtain the expression of the bulk EWCS. In particular, we utilize

the embedding space formalism to obtain the expression of the bulk EWCS which is given by the following geodesic length Eq. (81). As depicted in Fig. 7a, the endpoints of the bulk EWCS in this case involves a point on the a-brane and an arbitrary point on the RT surface homologous to the subsystem C. We consider these endpoints of the bulk EWCS as (a_2, z_{QES}, t) on the a-brane and $(R + r\sin(\phi), r\cos(\phi), t)$. Here ϕ is the angle defined to get the coordinates of the endpoint on the RT surface and R, r are defined in terms of the boundary coordinate as $\frac{p_2+p_3}{2}$, $\frac{p_3-p_2}{2}$ respectively. Therefore, the expression of the bulk EWCS can be obtained in this configuration using the Eq. (81) as

$$E_W = \frac{c}{3}\cosh^{-1}\left[\frac{z_h^2\left(\cosh\left(\frac{(R-a_2)}{z_h}\right)-1\right)}{r\ z_{\text{QES}}}\right], \tag{94}$$

where we considered that the bulk EWCS becomes minimum for $\phi = 0$. In the above equation, the z_{QES} may be obtained using the profile of the a-brane as $z_{\text{QES}} = z_h \sinh\left(\frac{a_2}{z_h}\right)$ with $k = 1$ [51]. Therefore, the expression of the EWCS becomes

$$E_W = \frac{c}{3}\log\left[\frac{\beta\left(\cosh\left(\frac{2\pi(R-a_2)}{\beta}\right)-1\right)}{\pi r \sinh\left(\frac{2\pi a_2}{\beta}\right)}\right]. \tag{95}$$

Note that the above result of the bulk EWCS exactly matches with the expression of the reflected entropy in Eq. (58) using Eq. (14).

Configuration-7

The contribution of the bulk EWCS in this configuration may be obtained by following the analogous analysis described in the previous case. As shown in Fig. 7b, the bulk EWCS now obtains contribution from the b-brane. However the computation of the bulk EWCS remains same as configuration-6, thus the expression of the EWCS may be given by

$$E_W = \frac{c}{3}\log\left[\frac{\beta\left(\cosh\left(\frac{2\pi(R-b_2)}{\beta}\right)-1\right)}{\pi r \sinh\left(\frac{2\pi b_2}{\beta}\right)}\right]. \tag{96}$$

Using Eq. (14), the above result matches with the replica technique result described in Eq. (62).

Configuration-8 and 9

In these configurations, the bulk EWCS may be obtained by following a similar procedure provided in the configurations-6. The only difference may be observed in the corresponding configurations arise from the enclosed entanglement wedge regions as depicted in Fig. 7c and d. Thus the expressions of the bulk EWCS in these cases are described by Eqs. (95) and (96) for the configurations 8 and 9 respectively.

Configuration-10

For the computation of the bulk EWCS in this configuration as shown in Fig. 8a, we utilize the embedding space formalism to express the length of the EWCS which is given by Eq. (81). Consequently, we obtain the corresponding length using the endpoints $(R + r\sin(\phi), r\cos(\phi), t)$ and $(R + r\sin(\phi), r\cos(\phi), -t + i\beta/2)$ of the bulk EWCS. Note that these endpoints of the EWCS are located on the RT surface homologous to subsystem C. Thus, The expression of the bulk EWCS may then be obtained as follows

$$E_W = \frac{c}{3}\log\left[\frac{\beta\cosh\left(\frac{2\pi t}{\beta}\right)}{\pi r}\right], \tag{97}$$

where r is related to the points p_2 and p_3 as $r = (p_3 - p_2)/2$. Above result matches with the replica technique result Eq. (67) of the reflected entropy by utilizing the proposal Eq. (14).

Configuration-11 and 12

As we can notice from the Fig. 8b and c that the bulk EWCS in these configurations is same as above case. However, the only observed difference in these configuration can be indicated from the enclosed entanglement wedge regions of the subsystem $A \cup B$. Therefore the expression of the bulk EWCS may be described by Eq. (97).

Configuration-13

We utilize the method discussed in the configuration-13 of the adjacent subsystems to compute the EWCS in this configuration described in Fig. 9a for the disjoint subsystems A and B. Consequently, we use Eq. (87) to obtain the expression of the EWCS for two disjoint subsystems. As depicted in Fig. 9a that the endpoints of the bulk EWCS are given as $((R + r\sin\phi)\cosh(\frac{2\pi t}{\beta}), (R + r\sin\phi)\sinh(\frac{2\pi t}{\beta}), r\cos\phi)$ and $(x_2, r_3\sinh(\frac{2\pi t}{\beta}), \sqrt{\left(r_3\cosh(\frac{2\pi t}{\beta})\right)^2 - x_2^2})$. Here ϕ is the angle defined to get the coordinates of the endpoint on the RT surface homologous to the subsystem C. Finally the expression of the bulk EWCS may be given by

$$E_W = \frac{c}{3}\log\left[\frac{\operatorname{sech}(\frac{2\pi t}{\beta})\sqrt{r^2+(R-r_2)^2}\sqrt{r^2+R^2+2Rr_2\cosh(\frac{4\pi t}{\beta})+r_2^2}}{r_2 r}\right], \tag{98}$$

where R, r are defined in terms of the boundary coordinates as $\frac{p_3+p_2}{2}$, $\frac{p_3-p_2}{2}$ respectively. In the above equation, we obtained the minimum length of the bulk EWCS for $\phi = 0$. Thus the corresponding result matches with the replica technique expression using the proposal Eq. (14).

Configuration-14

We may obtain the expression of the bulk EWCS in this configuration as shown in Fig. 9b by following a similar analysis described in the earlier configuration. Thus the expression of the bulk EWCS is given by

$$E_W = \frac{c}{3}\log\left[\frac{\operatorname{sech}(\frac{2\pi t}{\beta})\sqrt{r^2+(R-r_2)^2}\sqrt{r^2+R^2+2Rr_2\cosh(\frac{4\pi t}{\beta})+r_2^2}}{r_2 r}\right]. \tag{99}$$

Above expression matches with the replica technique result using the proposal Eq. (14).

Configuration-15 and 16

In these configurations, the bulk EWCS as depicted in Fig. 9c and d may be obtained by following a similar analysis discussed in configuration-13 and 14. The only difference in these configuration may be observed from the enclosed entanglement wedge region for the subsystem $A \cup B$. Therefore the bulk EWCS is given by Eqs. (88) and (89) for the configurations 15 and 16 respectively.

4 Markov gap

In this section, we will compare the behaviour of the profiles for the reflected entropy with that of the mutual information for the bipartite mixed states in three different cases where we will vary the subsystem sizes and the time. As mentioned in the introduction the difference between the holographic reflected entropy and the mutual information is described as the holographic Markov gap as defined in the context of quantum information theory and the Markov recovery process. To this end we first considered bipartite mixed states of adjacent subsystems in the reservoirs and obtained the profiles for the holographic reflected entropy by varying the size of the subsystem and time. Similarly, we described the corresponding holographic mutual information for these phases arising from the different structures of the RT surfaces supported by the subsystems. Subsequently we followed a similar analysis for the case of disjoint subsystems and in all the cases we demonstrated the behaviour of the holographic Markov gap described in [166].

4.1 Adjacent subsystems

We first consider adjacent subsystems A and B of finite lengths l_1 and l_2 respectively in both the TFD copies of the radiation reservoirs to describe the holographic Markov gap. In this context, the holographic mutual information for the adjacent subsystems A and B is defined as

$$I(A:B) = S(A) + S(B) - S(A \cup B), \tag{100}$$

where $S(X)$ is the holographic entanglement entropy of a subsystem X. We will investigate the qualitative nature of the holographic Markov gap for three different scenarios involving the subsystem sizes and time. For this purpose we will utilize the structure of the RT surfaces associated with the corresponding subsystems which was briefly described in [158] for the communicating black hole configurations.

(*i*) *Full system (**A** ∪ **B**) fixed, common point varied*

We first consider the case where the entire reservoir region is covered by the subsystem $A \cup B$ and the adjacent point is varied on a constant time slice. In this case, we obtained various phases of the holographic reflected entropy and the mutual information that characterizes the Markov gap as depicted in Fig. 10.

In the above figure, we observe different dominant contributions to the reflected entropy for two adjacent subsystems described in Sect. 3 while varying the common point. Specifically, the configurations (1), (10) and (2) for the two adjacent subsystems dominate in the consecutive phases of the reflected entropy in Fig. 10.

(*ii*) *Subsystem **A** fixed, **B** varied*

Next we consider the size of the subsystem A to be fixed on a constant time slice and analyzed the holographic Markov gap with the variation of the size of the subsystem B. We observed different phases of the reflected entropy and the mutual information to describe the Markov gap for each as shown in Fig. 11.

Similar to earlier case, we receive different dominant contributions corresponding to various configurations described in Sect. 3 to the reflected entropy while varying the size of the subsystem B. In particular, we observe configurations (5),and (1) dominate in the consecutive phase of the reflected entropy as shown in Fig. 11.

(*iii*) *Subsystems **A** and **B** fixed, time varied*

In this case, we fix both the size of the adjacent subsystems A and B and analyze the behaviour of the holographic Markov

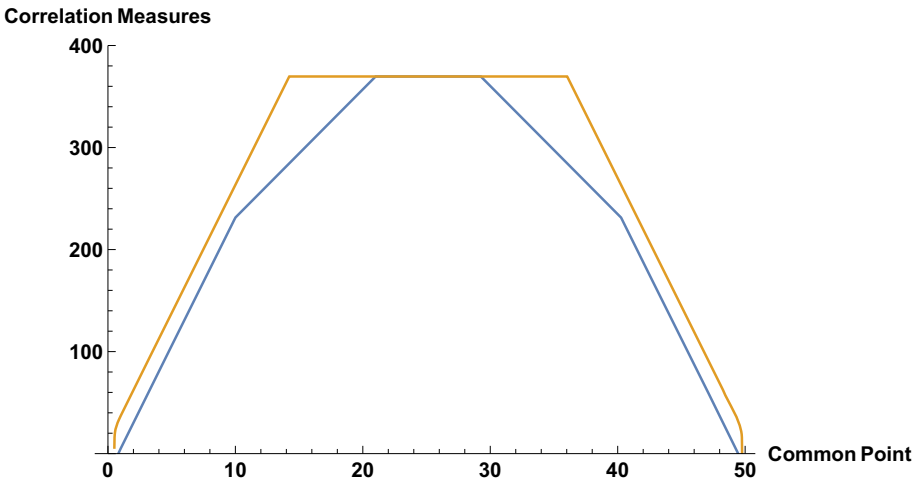

Fig. 10 Schematics shows the variation of the correlation measures reflected entropy (yellow) and mutual information (blue) for two adjacent subsystems A and B while the common boundary between them is being shifted in the radiation reservoirs. In the y-axis, the correlation measures are plotted with a scale factor of $\frac{6}{c}$ where c is the central charge of the CFT_2s located in the reservoirs and the Planck branes. Here $\beta = 1, t = 15, c = 500, \phi_0 = \frac{30c}{6}, \phi_r = \frac{30}{\pi}, L = \frac{16\pi}{\beta}, \epsilon = .001, A \cup B = [.01L, .99L]$

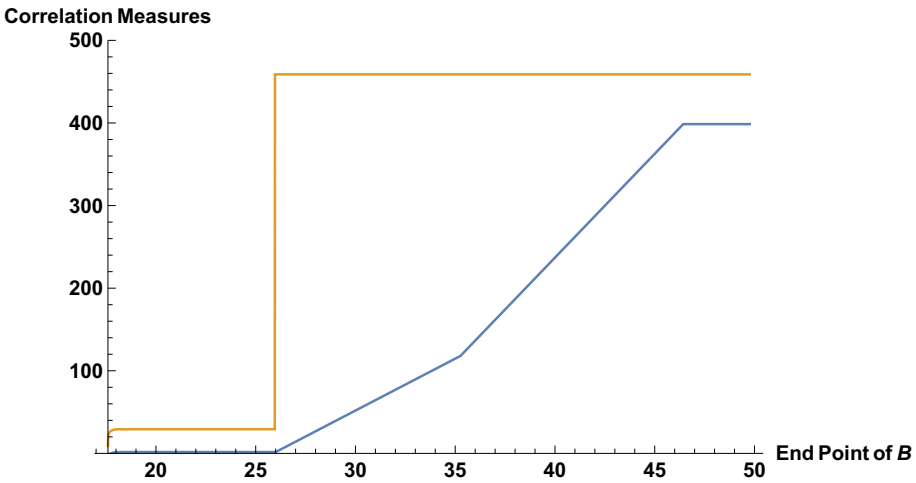

Fig. 11 Schematics shows the variation of the correlation measures namely, reflected entropy (yellow) and mutual information (blue) for two adjacent subsystems A and B with increasing size of the subsystem B in the radiation reservoirs. In the y-axis, the correlation measures are plotted with a scale factor of $\frac{6}{c}$ where c is the central charge of the CFT_2s located in the reservoirs and the Planck branes. Here $\beta = 1, t = 20, c = 500, \phi_0 = \frac{30c}{6}, \phi_r = \frac{30}{\pi}, L = \frac{16\pi}{\beta}, \epsilon = .001, A = [.01L, .15L]$

gap with time. In particular, we consider the equal lengths of the subsystems A and B Fig. 12.

Finally in the last case, we observe different dominant contributions (10) and (2) dominate consecutively in the reflected entropy for two adjacent subsystems as shown in Fig. 12.

4.2 Disjoint subsystems

We now consider a mixed state configuration of disjoint subsystems A and B where a subsystem C is sandwiched between them in both the TFD copies of the radiation reservoirs. Here we describe the holographic Markov gap in three different scenarios involving the subsystem sizes and the time. For the disjoint subsystems the mutual information is defined as

$$I(A:B) = S(A) + S(B) - S(A \cup B \cup C) - S(C), \quad (101)$$

where $S(X)$ is the holographic entanglement entropy of a subsystem X. Here we will utilize the structure of the RT surfaces associated with the subsystems in question which was again briefly described in [158] for the communicating black hole scenarios.

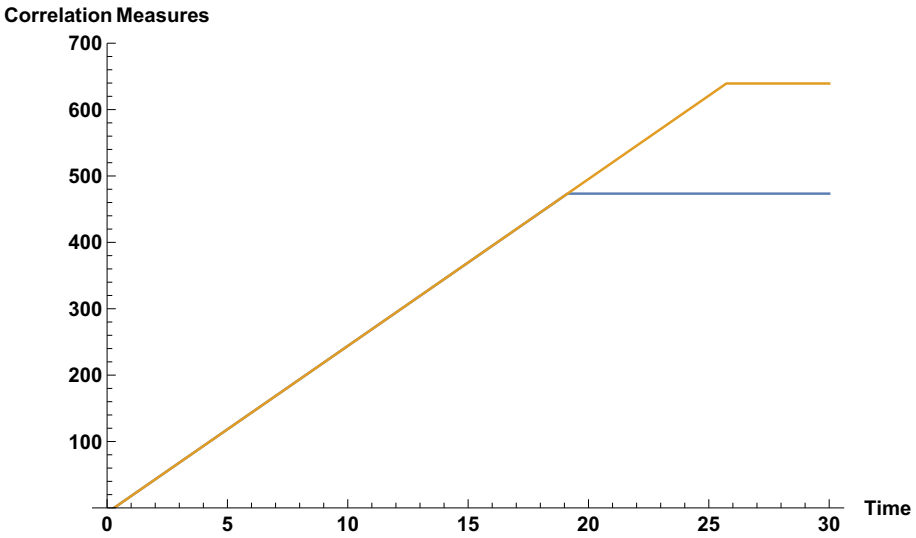

Fig. 12 Schematics shows the variation of the correlation measures namely, reflected entropy (yellow) and mutual information (blue) for two adjacent subsystems A and B while increasing the time t. In the y-axis, the correlation measures are plotted with a scale factor of $\frac{6}{c}$ where c is the central charge of the CFT_2s located in the reservoirs and the Planck branes. Here $\beta = 1$, $c = 500$, $\phi_0 = \frac{30c}{6}$, $\phi_r = \frac{30}{\pi}$, $L = \frac{16\pi}{\beta}$, $\epsilon = .001$, $A = [.01L, .5L]$ and $B = [.5L, .99L]$

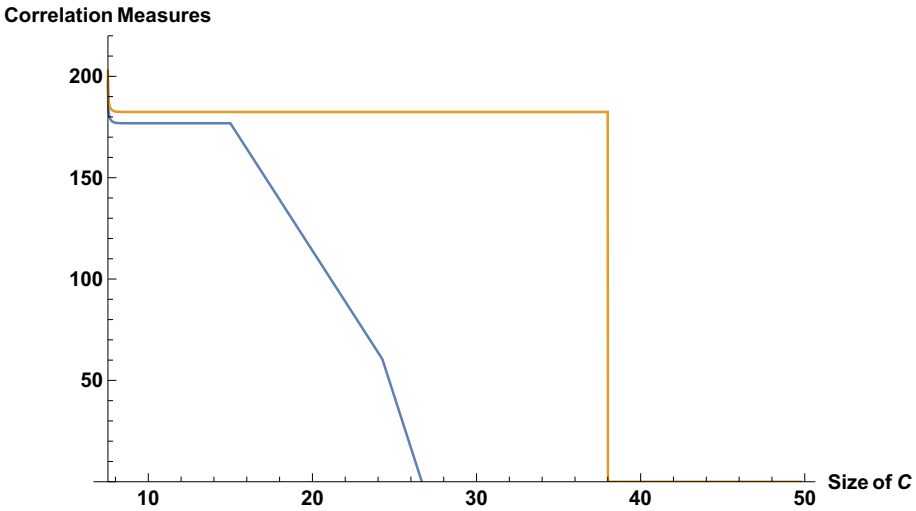

Fig. 13 Schematics shows the variation of the correlation measures namely, reflected entropy (yellow) and mutual information (blue) for two disjoint subsystems A and B while increasing common point. In the y-axis, the correlation measures are plotted with a scale factor of $\frac{6}{c}$ where c is the central charge of the CFT_2s located in the reservoirs and the Planck branes. Here $\beta = 1$, $c = 500$, $\phi_0 = \frac{30c}{6}$, $\phi_r = \frac{30}{\pi}$, $L = \frac{16\pi}{\beta}$, $\epsilon = .001$ and $A = [.01L, .15L]$

(*i*) *Subsystem* ***A*** *fixed,* ***C*** *varied*

In this case, we fix the size of the subsystem A and gradually vary the size of the subsystem C on a constant time slice. We analyze the behavior of the holographic Markov gap from the comparison between the reflected entropy described in Sect. 3 and the mutual information in Eq. (101). We observe different phases of the holographic Markov gap as shown in Fig. 13.

In this case, we receive different dominant contributions for various configurations described in Sect. 3 to the reflected entropy for two disjoint subsystems while varying the size of the subsystem C. We observe contribution (1) dominates in the starting phase of the reflected entropy as shown in Fig. 13.

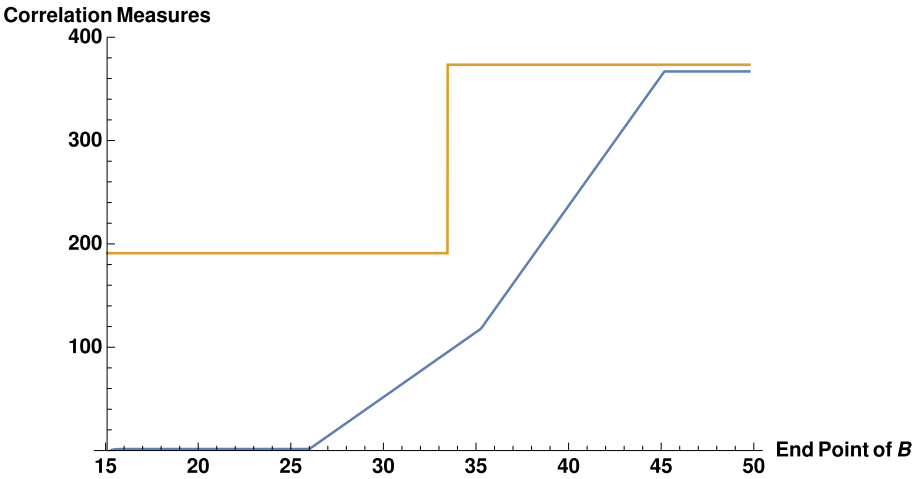

Fig. 14 Schematics shows the variation of the correlation measures namely, reflected entropy (yellow) and mutual information (blue) for two disjoint subsystems A and B while increasing the size of the subsystem B. In the y-axis, the correlation measures are plotted with a scale factor of $\frac{6}{c}$ where c is the central charge of the CFT_2s located in the reservoirs and the Planck branes. Here $\beta = 1$, $c = 500$, $\phi_0 = \frac{30c}{6}$, $\phi_r = \frac{30}{\pi}$, $L = \frac{16\pi}{\beta}$, $\epsilon = .001$, $A = [.01L, .15L]$ and $C = [.15L, .30L]$

(*ii*) *Subsystems* ***A*** *and* ***C*** *fixed,* ***B***

Next we consider the size of the subsystems A and C to be fixed on a constant time slice and analyze the behavior of the holographic Markov gap while varying the size of the subsystem B. We obtained various phases of the reflected entropy and the mutual information as described in Fig. 14.

As earlier, we note that the reflected entropy curve in Fig. 14 is dominated by various contributions from the configurations describe in Sect. 3. Particularly, configurations (5) and (1) of the reflected entropy for the disjoint subsystems dominate the corresponding phases shown in Fig. 14.

(*iii*) *Subsystems* ***A***, ***B*** *and* ***C*** *fixed, time varied*

Finally in the last case, we considered equal sizes of the subsystems A and B on a constant time slice and observed various phases of the holographic Markov gap through the analysis of the reflected entropy as obtained in Sect. 3 and the mutual information in eq. (101) with the variation of the time as shown in Fig. 15.

Once again in the last scenario, the reflected entropy for the two disjoint subsystems receives different dominant contributions from the configurations described in Sect. 3 with increasing time t. Specifically, the configurations (10) and (2) for the two disjoint subsystems dominate respectively in the consecutive phases of the reflected entropy depicted by the yellow curve in Fig. 15.

5 Summary and discussion

To summarize, we have computed the reflected entropy for various bipartite mixed states described by adjacent and disjoint subsystems at a finite temperature for the communicating black hole configurations in a Planck brane world geometry. In this context, we considered a configuration involving two eternal JT black holes with two finite sized radiation reservoirs coupled to two quantum dots. The bulk dual of the corresponding configuration was described by an eternal AdS_3 BTZ black hole geometry truncated by two Planck branes. Interestingly, the gravitating nature of each of the radiation reservoirs corresponding to the two Planck branes could be demonstrated from the perspective of the other brane. Note that for this configuration the two dimensional eternal JT black holes are located on the Planck branes with a single matter CFT_2 described on the entire geometry with transparent boundary conditions imposed at the interfaces of the radiation reservoirs and the Planck branes.

The reflected entropy for the mixed state configurations in question was computed for the communicating black hole configuration described above. We demonstrated the different possible dominant channels for the multipoint twist correlators involved in the computation of the reflected entropy in the large central charge limit. In this context, we first investigated the reflected entropy in the large central charge limit for two adjacent subsystems located in the radiation reservoirs utilizing the replica technique developed in [136]. Subsequently, we followed a similar analysis for the computation of the reflected entropy of two disjoint subsystems located in the radiation reservoirs. These field theory replica technique results were substantiated by explicit bulk holographic computation of the EWCS in the dual brane world geometry.

Furthermore, we also analyzed the holographic Markov gap as described in [166] between the reflected entropy and the mutual information for various bipartite mixed states in the context of AdS_3/CFT_2 correspondence. In this connec-

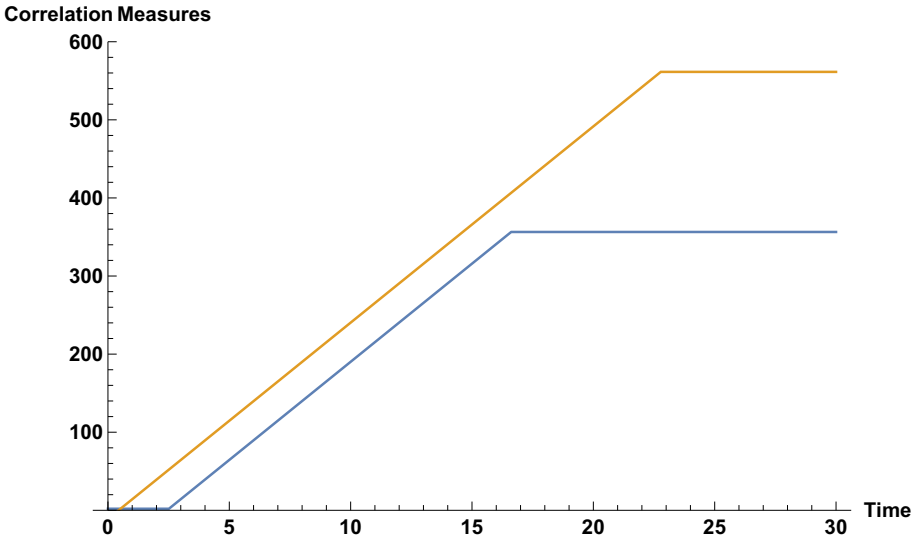

Fig. 15 Schematics shows the variation of the correlation measures namely, reflected entropy (yellow) and mutual information (blue) for two disjoint subsystems A and B while varying the time t. In the y-axis, the correlation measures are plotted with a scale factor of $\frac{6}{c}$ where c is the central charge of the CFT_2s located in the reservoirs and the Planck branes. Here $\beta = 1$, $c = 500$, $\phi_0 = \frac{30c}{6}$, $\phi_r = \frac{30}{\pi}$, $L = \frac{16\pi}{\beta}$, $\epsilon = .001$, $A = [.01L, .45L]$, $C = [.45L, .55L]$ and $B = [.55L, .99L]$

tion, we compared the holographic reflected entropy and the mutual information for various bipartite mixed state configurations under consideration. We obtained different profiles of the holographic Markov gap in various configurations related to the variation of size of the subsystems and time.

There are various fascinating future directions which can be investigated to obtain a better understanding of the mixed state entanglement structure in Hawking radiation. Following some recent developments in [158,177,178], it will be interesting to study other mixed state correlation measures and their corresponding Markov gaps. One may also extend the study of the present article to investigate the multipartite correlations where it is expected to observe the characteristics of the holographic Markov gap. We would like to address some these interesting issues in the near future.

Acknowledgements The research work of JKB is supported by the grant 110-2636-M-110-008 by the National Science and Technology Council (NSTC) of Taiwan. The work of GS is partially supported by the Dr. Jagmohan Garg Chair Professor position at the Indian Institute of Technology, Kanpur.

Data Availability Statement This manuscript has no associated data or the data will not be deposited. [Authors' comment: This manuscript has no associated data.]

Open Access This article is licensed under a Creative Commons Attribution 4.0 International License, which permits use, sharing, adaptation, distribution and reproduction in any medium or format, as long as you give appropriate credit to the original author(s) and the source, provide a link to the Creative Commons licence, and indicate if changes were made. The images or other third party material in this article are included in the article's Creative Commons licence, unless indicated otherwise in a credit line to the material. If material is not included in the article's Creative Commons licence and your intended use is not permitted by statutory regulation or exceeds the permitted use, you will need to obtain permission directly from the copyright holder. To view a copy of this licence, visit http://creativecommons.org/licenses/by/4.0/.
Funded by SCOAP[3].

References

1. S.W. Hawking, Particle creation by black holes. Commun. Math. Phys. **43**, 199–220 (1975). https://doi.org/10.1007/BF02345020
2. S.W. Hawking, Breakdown of predictability in gravitational collapse. Phys. Rev. D **14**, 2460–2473 (1976). https://doi.org/10.1103/PhysRevD.14.2460
3. D.N. Page, Information in black hole radiation. Phys. Rev. Lett. **71**, 3743–3746 (1993). https://doi.org/10.1103/PhysRevLett.71.3743. arXiv:hep-th/9306083
4. A. Almheiri, N. Engelhardt, D. Marolf, H. Maxfield, The entropy of bulk quantum fields and the entanglement wedge of an evaporating black hole. JHEP **12**, 063 (2019). https://doi.org/10.1007/JHEP12(2019)063. arXiv:1905.08762
5. G. Penington, Entanglement wedge reconstruction and the information paradox. JHEP **09**, 002 (2020). https://doi.org/10.1007/JHEP09(2020)002. arXiv:1905.08255
6. S. Ryu, T. Takayanagi, Holographic derivation of entanglement entropy from AdS/CFT. Phys. Rev. Lett. **96**, 181602 (2006). https://doi.org/10.1103/PhysRevLett.96.181602. arXiv:hep-th/0603001
7. S. Ryu, T. Takayanagi, Aspects of holographic entanglement entropy. JHEP **08**, 045 (2006). https://doi.org/10.1088/1126-6708/2006/08/045. arXiv:hep-th/0605073
8. V.E. Hubeny, M. Rangamani, T. Takayanagi, A covariant holographic entanglement entropy proposal. JHEP **07**, 062 (2007). https://doi.org/10.1088/1126-6708/2007/07/062. arXiv:0705.0016

9. T. Faulkner, A. Lewkowycz, J. Maldacena, Quantum corrections to holographic entanglement entropy. JHEP **11**, 074 (2013). https://doi.org/10.1007/JHEP11(2013)074. arXiv:1307.2892
10. N. Engelhardt, A.C. Wall, Quantum extremal surfaces: holographic entanglement entropy beyond the classical regime. JHEP **01**, 073 (2015). https://doi.org/10.1007/JHEP01(2015)073. arXiv:1408.3203
11. A. Almheiri, R. Mahajan, J. Maldacena, Y. Zhao, The Page curve of Hawking radiation from semiclassical geometry. JHEP **03**, 149 (2020). https://doi.org/10.1007/JHEP03(2020)149. arXiv:1908.10996
12. A. Almheiri, T. Hartman, J. Maldacena, E. Shaghoulian, A. Tajdini, The entropy of Hawking radiation. Rev. Mod. Phys. **93**, 035002 (2021). https://doi.org/10.1103/RevModPhys.93.035002. arXiv:2006.06872
13. A. Almheiri, R. Mahajan, J. Maldacena, Islands outside the horizon. arXiv:1910.11077
14. M. Miyaji, T. Takayanagi, T. Ugajin, Spectrum of end of the world branes in holographic BCFTs. JHEP **06**, 023 (2021). https://doi.org/10.1007/JHEP06(2021)023. arXiv:2103.06893
15. M. Miyaji, Island for gravitationally prepared state and pseudo entanglement wedge. JHEP **12**, 013 (2021). https://doi.org/10.1007/JHEP12(2021)013. arXiv:2109.03830
16. M. Miyaji, C. Murdia, Holographic BCFT with a defect on the end-of-the-world brane. JHEP **11**, 123 (2022). https://doi.org/10.1007/JHEP11(2022)123. arXiv:2208.13783
17. A. Almheiri, R. Mahajan, J.E. Santos, Entanglement islands in higher dimensions. SciPost Phys. **9**, 001 (2020). https://doi.org/10.21468/SciPostPhys.9.1.001. arXiv:1911.09666
18. L. Anderson, O. Parrikar, R.M. Soni, Islands with gravitating baths: towards ER = EPR. JHEP **21**, 226 (2020). https://doi.org/10.1007/JHEP10(2021)226. arXiv:2103.14746
19. Y. Chen, Pulling out the island with modular flow. JHEP **03**, 033 (2020). https://doi.org/10.1007/JHEP03(2020)033. arXiv:1912.02210
20. V. Balasubramanian, A. Kar, O. Parrikar, G. Sárosi, T. Ugajin, Geometric secret sharing in a model of Hawking radiation. JHEP **01**, 177 (2021). https://doi.org/10.1007/JHEP01(2021)177. arXiv:2003.05448
21. Y. Chen, X.-L. Qi, P. Zhang, Replica wormhole and information retrieval in the SYK model coupled to Majorana chains. JHEP **06**, 121 (2020). https://doi.org/10.1007/JHEP06(2020)121. arXiv:2003.13147
22. F.F. Gautason, L. Schneiderbauer, W. Sybesma, L. Thorlacius, Page curve for an evaporating black hole. JHEP **05**, 091 (2020). https://doi.org/10.1007/JHEP05(2020)091. arXiv:2004.00598
23. A. Bhattacharya, Multipartite purification, multiboundary wormholes, and islands in AdS_3/CFT_2. Phys. Rev. D **102**, 046013 (2020). https://doi.org/10.1103/PhysRevD.102.046013. arXiv:2003.11870
24. T. Anegawa, N. Iizuka, Notes on islands in asymptotically flat 2d dilaton black holes. JHEP **07**, 036 (2020). https://doi.org/10.1007/JHEP07(2020)036. arXiv:2004.01601
25. K. Hashimoto, N. Iizuka, Y. Matsuo, Islands in Schwarzschild black holes. JHEP **06**, 085 (2020). https://doi.org/10.1007/JHEP06(2020)085. arXiv:2004.05863
26. T. Hartman, E. Shaghoulian, A. Strominger, Islands in asymptotically flat 2D gravity. JHEP **07**, 022 (2020). https://doi.org/10.1007/JHEP07(2020)022. arXiv:2004.13857
27. C. Krishnan, V. Patil, J. Pereira, Page curve and the information paradox in flat space. arXiv:2005.02993
28. M. Alishahiha, A. Faraji Astaneh, A. Naseh, Island in the presence of higher derivative terms. JHEP **02**, 035 (2021). https://doi.org/10.1007/JHEP02(2021)035. arXiv:2005.08715
29. H. Geng, A. Karch, Massive islands. JHEP **09**, 121 (2020). https://doi.org/10.1007/JHEP09(2020)121. arXiv:2006.02438
30. T. Li, J. Chu, Y. Zhou, Reflected entropy for an evaporating black hole. JHEP **11**, 155 (2020). https://doi.org/10.1007/JHEP11(2020)155. arXiv:2006.10846
31. V. Chandrasekaran, M. Miyaji, P. Rath, Including contributions from entanglement islands to the reflected entropy. Phys. Rev. D **102**, 086009 (2020). https://doi.org/10.1103/PhysRevD.102.086009. arXiv:2006.10754
32. D. Bak, C. Kim, S.-H. Yi, J. Yoon, Unitarity of entanglement and islands in two-sided Janus black holes. JHEP **01**, 155 (2021). https://doi.org/10.1007/JHEP01(2021)155. arXiv:2006.11717
33. C. Krishnan, Critical islands. JHEP **01**, 179 (2021). https://doi.org/10.1007/JHEP01(2021)179. arXiv:2007.06551
34. A. Karlsson, Replica wormhole and island incompatibility with monogamy of entanglement. arXiv:2007.10523
35. T. Hartman, Y. Jiang, E. Shaghoulian, Islands in cosmology. JHEP **11**, 111 (2020). https://doi.org/10.1007/JHEP11(2020)111. arXiv:2008.01022
36. V. Balasubramanian, A. Kar, T. Ugajin, Entanglement between two disjoint universes. JHEP **02**, 136 (2021). https://doi.org/10.1007/JHEP02(2021)136. arXiv:2008.05274
37. V. Balasubramanian, A. Kar, T. Ugajin, Islands in de Sitter space. JHEP **02**, 072 (2021). https://doi.org/10.1007/JHEP02(2021)072. arXiv:2008.05275
38. W. Sybesma, Pure de Sitter space and the island moving back in time. Class. Quantum Gravity **38**, 145012 (2021). https://doi.org/10.1088/1361-6382/abff9a. arXiv:2008.07994
39. H.Z. Chen, R.C. Myers, D. Neuenfeld, I.A. Reyes, J. Sandor, Quantum extremal islands made easy. Part II: black holes on the brane. JHEP **12**, 025 (2020). https://doi.org/10.1007/JHEP12(2020)025. arXiv:2010.00018
40. Y. Ling, Y. Liu, Z.-Y. Xian, Island in charged black holes. JHEP **03**, 251 (2021). https://doi.org/10.1007/JHEP03(2021)251. arXiv:2010.00037
41. J. Hernandez, R.C. Myers, S.-M. Ruan, Quantum extremal islands made easy. Part III. Complexity on the brane. JHEP **02**, 173 (2021). https://doi.org/10.1007/JHEP02(2021)173. arXiv:2010.16398
42. D. Marolf, H. Maxfield, Observations of Hawking radiation: the Page curve and baby universes. JHEP **04**, 272 (2021). https://doi.org/10.1007/JHEP04(2021)272. arXiv:2010.06602
43. Y. Matsuo, Islands and stretched horizon. JHEP **07**, 051 (2021). https://doi.org/10.1007/JHEP07(2021)051. arXiv:2011.08814
44. I. Akal, Y. Kusuki, N. Shiba, T. Takayanagi, Z. Wei, Entanglement entropy in a holographic moving mirror and the page curve. Phys. Rev. Lett. **126**, 061604 (2021). https://doi.org/10.1103/PhysRevLett.126.061604. arXiv:2011.12005
45. E. Caceres, A. Kundu, A.K. Patra, S. Shashi, Warped information and entanglement islands in AdS/WCFT. JHEP **07**, 004 (2021). https://doi.org/10.1007/JHEP07(2021)004. arXiv:2012.05425
46. S. Raju, Lessons from the information paradox. Phys. Rep. **943**, 2187 (2022). https://doi.org/10.1016/j.physrep.2021.10.001. arXiv:2012.05770
47. F. Deng, J. Chu, Y. Zhou, Defect extremal surface as the holographic counterpart of Island formula. JHEP **03**, 008 (2021). https://doi.org/10.1007/JHEP03(2021)008. arXiv:2012.07612
48. T. Anous, M. Meineri, P. Pelliconi, J. Sonner, Sailing past the end of the world and discovering the island. arXiv:2202.11718
49. R. Bousso, E. Wildenhain, Islands in closed and open universes. arXiv:2202.05278
50. Q.-L. Hu, D. Li, R.-X. Miao, Y.-Q. Zeng, AdS/BCFT and Island for curvature-squared gravity. arXiv:2202.03304
51. G. Grimaldi, J. Hernandez, R.C. Myers, Quantum extremal islands made easy, part IV: massive black holes on the brane. arXiv:2202.00679
52. C. Akers, T. Faulkner, S. Lin, P. Rath, The page curve for reflected entropy. arXiv:2201.11730

53. M.-H. Yu, C.-Y. Lu, X.-H. Ge, S.-J. Sin, Island, page curve and superradiance of rotating BTZ black holes. arXiv:2112.14361
54. H. Geng, A. Karch, C. Perez-Pardavila, S. Raju, L. Randall, M. Riojas et al., Entanglement phase structure of a holographic bcft in a black hole background. arXiv:2112.09132
55. C.-J. Chou, H. B. Lao, Y. Yang, Page curve of effective hawking radiation. arXiv:2111.14551
56. T.J. Hollowood, S.P. Kumar, A. Legramandi, N. Talwar, Grey-body Factors, irreversibility and multiple island saddles. arXiv:2111.02248
57. S. He, Y. Sun, L. Zhao, Y.-X. Zhang, The universality of islands outside the horizon, arXiv:2110.07598
58. I. Aref'eva, I. Volovich, A note on islands in Schwarzschild black holes. arXiv:2110.04233
59. Y. Ling, P. Liu, Y. Liu, C. Niu, Z.-Y. Xian, C.-Y. Zhang, Reflected entropy in double holography. JHEP **02**, 037 (2022). https://doi.org/10.1007/JHEP02(2022)037. arXiv:2109.09243
60. A. Bhattacharya, A. Bhattacharyya, P. Nandy, A.K. Patra, Partial islands and subregion complexity in geometric secret-sharing model. JHEP **12**, 091 (2021). https://doi.org/10.1007/JHEP12(2021)091. arXiv:2109.07842
61. S. Azarnia, R. Fareghbal, A. Naseh, H. Zolfi, Islands in flat-space cosmology. Phys. Rev. D **104**, 126017 (2021). https://doi.org/10.1103/PhysRevD.104.126017. arXiv:2109.04795
62. A. Saha, S. Gangopadhyay, J.P. Saha, Mutual information, islands in black holes and the Page curve. arXiv:2109.02996
63. T.J. Hollowood, S.P. Kumar, A. Legramandi, N. Talwar, Ephemeral islands, plunging quantum extremal surfaces and BCFT channels. JHEP **01**, 078 (2022). https://doi.org/10.1007/JHEP01(2022)078. arXiv:2109.01895
64. P.-C. Sun, Entanglement islands from holographic thermalization of rotating charged black hole. arXiv:2108.12557
65. T. Li, M.-K. Yuan, Y. Zhou, Defect extremal surface for reflected entropy. JHEP **01**, 018 (2022). https://doi.org/10.1007/JHEP01(2022)018. arXiv:2108.08544
66. S.E. Aguilar-Gutierrez, A. Chatwin-Davies, T. Hertog, N. Pinzani-Fokeeva, B. Robinson, Islands in multiverse models. JHEP **11**, 212 (2021). https://doi.org/10.1007/JHEP11(2021)212. arXiv:2108.01278
67. B. Ahn, S.-E. Bak, H.-S. Jeong, K.-Y. Kim, Y.-W. Sun, Islands in charged linear dilaton black holes. Phys. Rev. D **105**, 046012 (2022). https://doi.org/10.1103/PhysRevD.105.046012. arXiv:2107.07444
68. M.-H. Yu, X.-H. Ge, Islands and Page curves in charged dilaton black holes. Eur. Phys. J. C **82**, 14 (2022). https://doi.org/10.1140/epjc/s10052-021-09932-w. arXiv:2107.03031
69. Y. Lu, J. Lin, Islands in Kaluza–Klein black holes. Eur. Phys. J. C **82**, 132 (2022). https://doi.org/10.1140/epjc/s10052-022-10074-w. arXiv:2106.07845
70. E. Caceres, A. Kundu, A. K. Patra, S. Shashi, Page curves and bath deformations. arXiv:2107.00022
71. I. Akal, Y. Kusuki, N. Shiba, T. Takayanagi, Z. Wei, Holographic moving mirrors. Class. Quantum Gravity **38**, 224001 (2021). https://doi.org/10.1088/1361-6382/ac2c1b. arXiv:2106.11179
72. I. Aref'eva, T. Rusalev, I. Volovich, Entanglement entropy of near-extremal black hole. arXiv:2202.10259
73. I. Aref'eva, I. Volovich, Complete evaporation of black holes and page curves. arXiv:2202.00548
74. R. Bousso, X. Dong, N. Engelhardt, T. Faulkner, T. Hartman, S.H. Shenker et al., Snowmass white paper: quantum aspects of black holes and the emergence of spacetime. arXiv:2201.03096
75. C. Krishnan, V. Mohan, Interpreting the bulk page curve: a vestige of locality on holographic screens. arXiv:2112.13783
76. D.-F. Zeng, Spontaneous radiation of black holes. arXiv:2112.12531
77. D. Teresi, Islands and the de Sitter entropy bound. arXiv:2112.03922
78. K. Okuyama, K. Sakai, Page curve from dynamical branes in JT gravity. JHEP **02**, 087 (2022). https://doi.org/10.1007/JHEP02(2022)087. arXiv:2111.09551
79. P. Chen, M. Sasaki, D.-H. Yeom, J. Yoon, Solving information loss paradox via Euclidean path integral. arXiv:2111.01005
80. J.F. Pedraza, A. Svesko, W. Sybesma, M.R. Visser, Microcanonical action and the entropy of hawking radiation. arXiv:2111.06912
81. B. Guo, M.R.R. Hughes, S.D. Mathur, M. Mehta, Contrasting the fuzzball and wormhole paradigms for black holes. Turk. J. Phys. **45**, 281–365 (2021). https://doi.org/10.3906/fiz-2111-13. arXiv:2111.05295
82. T. Kibe, P. Mandayam, A. Mukhopadhyay, Holographic spacetime, black holes and quantum error correcting codes: a review. arXiv:2110.14669
83. R. Renner, J. Wang, The black hole information puzzle and the quantum de Finetti theorem. arXiv:2110.14653
84. X. Dong, S. McBride, W.W. Weng, Replica wormholes and holographic entanglement negativity. arXiv:2110.11947
85. S. Raju, Failure of the split property in gravity and the information paradox. arXiv:2110.05470
86. C.H. Nam, Entanglement entropy and Page curve of black holes with island in massive gravity. arXiv:2108.10144
87. J. Kames-King, E. Verheijden, E. Verlinde, No page curves for the de Sitter Horizon. arXiv:2108.09318
88. B. Chen, B. Czech, Z.-Z. Wang, Quantum information in holographic duality. arXiv:2108.09188
89. Y. Sato, Complexity in a moving mirror model. arXiv:2108.04637
90. J. Kudler-Flam, V. Narovlansky, S. Ryu, Distinguishing random and black hole microstates. PRX Quantum **2**, 040340 (2021). https://doi.org/10.1103/PRXQuantum.2.040340. arXiv:2108.00011
91. H. Geng, S. Lüst, R.K. Mishra, D. Wakeham, Holographic BCFTs and communicating black holes. JHEP **08**, 003 (2021). https://doi.org/10.1007/JHEP08(2021)003. arXiv:2104.07039
92. X. Wang, K. Zhang, J. Wang, What can we learn about islands and state paradox from quantum information theory? arXiv:2107.09228
93. D.S. Ageev, Shaping contours of entanglement islands in BCFT. arXiv:2107.09083
94. L. Buoninfante, F. Di Filippo, S. Mukohyama, On the assumptions leading to the information loss paradox. JHEP **10**, 081 (2021). https://doi.org/10.1007/JHEP10(2021)081. arXiv:2107.05662
95. M. Cadoni, A.P. Sanna, Unitarity and page curve for evaporation of 2D AdS black holes. arXiv:2106.14738
96. D. Marolf, H. Maxfield, The page curve and baby universes. Int. J. Mod. Phys. D **30**, 2142027 (2021). https://doi.org/10.1142/S021827182142027X. arXiv:2105.12211
97. J. Chu, F. Deng, Y. Zhou, Page curve from defect extremal surface and island in higher dimensions. JHEP **10**, 149 (2021). https://doi.org/10.1007/JHEP10(2021)149. arXiv:2105.09106
98. E.Y. Urbach, The entanglement entropy of typical pure states and replica wormholes. JHEP **12**, 125 (2021). https://doi.org/10.1007/JHEP12(2021)125. arXiv:2105.15059
99. R. Li, X. Wang, J. Wang, Island may not save the information paradox of Liouville black holes. Phys. Rev. D **104**, 106015 (2021). https://doi.org/10.1103/PhysRevD.104.106015. arXiv:2105.03271
100. D. Neuenfeld, Homology conditions for RT surfaces in double holography. arXiv:2105.01130
101. L. Aalsma, W. Sybesma, The price of curiosity: information recovery in de Sitter space. JHEP **05**, 291 (2021). https://doi.org/10.1007/JHEP05(2021)291. arXiv:2104.00006

102. K. Ghosh, C. Krishnan, Dirichlet baths and the not-so-fine-grained Page curve. JHEP **08**, 119 (2021). https://doi.org/10.1007/JHEP08(2021)119. arXiv:2103.17253
103. A. Bhattacharya, A. Bhattacharyya, P. Nandy, A.K. Patra, Islands and complexity of eternal black hole and radiation subsystems for a doubly holographic model. JHEP **05**, 135 (2021). https://doi.org/10.1007/JHEP05(2021)135. arXiv:2103.15852
104. H. Geng, Y. Nomura, H.-Y. Sun, Information paradox and its resolution in de Sitter holography. Phys. Rev. D **103**, 126004 (2021). https://doi.org/10.1103/PhysRevD.103.126004. arXiv:2103.07477
105. C. Krishnan, V. Mohan, Hints of gravitational ergodicity: Berry's ensemble and the universality of the semi-classical Page curve. JHEP **05**, 126 (2021). https://doi.org/10.1007/JHEP05(2021)126. arXiv:2102.07703
106. E. Verheijden, E. Verlinde, From the BTZ black hole to JT gravity: geometrizing the island. JHEP **11**, 092 (2021). https://doi.org/10.1007/JHEP11(2021)092. arXiv:2102.00922
107. R. Bousso, A. Shahbazi-Moghaddam, Island finder and entropy bound. Phys. Rev. D **103**, 106005 (2021). https://doi.org/10.1103/PhysRevD.103.106005. arXiv:2101.11648
108. G.K. Karananas, A. Kehagias, J. Taskas, Islands in linear dilaton black holes. JHEP **03**, 253 (2021). https://doi.org/10.1007/JHEP03(2021)253. arXiv:2101.00024
109. K. Goto, T. Hartman, A. Tajdini, Replica wormholes for an evaporating 2D black hole. JHEP **04**, 289 (2021). https://doi.org/10.1007/JHEP04(2021)289. arXiv:2011.09043
110. A. Bhattacharya, A. Chanda, S. Maulik, C. Northe, S. Roy, Topological shadows and complexity of islands in multiboundary wormholes. JHEP **02**, 152 (2021). https://doi.org/10.1007/JHEP02(2021)152. arXiv:2010.04134
111. H.Z. Chen, Z. Fisher, J. Hernandez, R.C. Myers, S.-M. Ruan, Evaporating black holes coupled to a thermal bath. JHEP **01**, 065 (2021). https://doi.org/10.1007/JHEP01(2021)065. arXiv:2007.11658
112. C.A. Agón, S.F. Lokhande, J.F. Pedraza, Local quenches, bulk entanglement entropy and a unitary Page curve. JHEP **08**, 152 (2020). https://doi.org/10.1007/JHEP08(2020)152. arXiv:2004.15010
113. A. Laddha, S.G. Prabhu, S. Raju, P. Shrivastava, The holographic nature of null infinity. SciPost Phys. **10**, 041 (2021). https://doi.org/10.21468/SciPostPhys.10.2.041. arXiv:2002.02448
114. C. Akers, N. Engelhardt, D. Harlow, Simple holographic models of black hole evaporation. JHEP **08**, 032 (2020). https://doi.org/10.1007/JHEP08(2020)032. arXiv:1910.00972
115. H.Z. Chen, Z. Fisher, J. Hernandez, R.C. Myers, S.-M. Ruan, Information flow in black hole evaporation. JHEP **03**, 152 (2020). https://doi.org/10.1007/JHEP03(2020)152. arXiv:1911.03402
116. D. Basu, H. Parihar, V. Raj, G. Sengupta, Defect extremal surfaces for entanglement negativity. arXiv:2205.07905
117. C.F. Uhlemann, Islands and Page curves in 4d from Type IIB. JHEP **08**, 104 (2021). https://doi.org/10.1007/JHEP08(2021)104. arXiv:2105.00008
118. C.F. Uhlemann, Information transfer with a twist. JHEP **01**, 126 (2022). https://doi.org/10.1007/JHEP01(2022)126. arXiv:2111.11443
119. C. Germani, Retrieving black hole information from the main Lorentzian saddle point. arXiv:2204.13046
120. G. Yadav, Page curves of Reissner–Nordström black hole in HD gravity. arXiv:2204.11882
121. F. Omidi, Entropy of Hawking radiation for two-sided hyperscaling violating black branes. JHEP **04**, 022 (2022). https://doi.org/10.1007/JHEP04(2022)022. arXiv:2112.05890
122. G. Yadav, A. Misra, ("Swiss-Cheese") Entanglement entropy when Page-ing $\mathcal{M}$ theory dual of thermal QCD above T_c at intermediate coupling. arXiv:2207.04048
123. H.Z. Chen, R.C. Myers, D. Neuenfeld, I.A. Reyes, J. Sandor, Quantum extremal islands made easy. Part I: entanglement on the brane. JHEP **10**, 166 (2020). https://doi.org/10.1007/JHEP10(2020)166. arXiv:2006.04851
124. G. Yadav, Multiverse in Karch–Randall braneworld. arXiv:2301.06151
125. G. Penington, S.H. Shenker, D. Stanford, Z. Yang, Replica wormholes and the black hole interior. arXiv:1911.11977
126. A. Almheiri, T. Hartman, J. Maldacena, E. Shaghoulian, A. Tajdini, Replica wormholes and the entropy of hawking radiation. JHEP **05**, 013 (2020). https://doi.org/10.1007/JHEP05(2020)013. arXiv:1911.12333
127. R. Jackiw, Lower dimensional gravity. Nucl. Phys. B **252**, 343–356 (1985). https://doi.org/10.1016/0550-3213(85)90448-1
128. C. Teitelboim, Gravitation and Hamiltonian structure in two space-time dimensions. Phys. Lett. B **126**, 41–45 (1983). https://doi.org/10.1016/0370-2693(83)90012-6
129. S. Sachdev, J. Ye, Gapless spin fluid ground state in a random, quantum Heisenberg magnet. Phys. Rev. Lett. **70**, 3339 (1993). https://doi.org/10.1103/PhysRevLett.70.3339. arXiv:cond-mat/9212030
130. A. Kitaev, A simple model of quantum holography. Talks at KITP, April 7, 2015 and May 27, 2015. http://online.kitp.ucsb.edu/online/entangled15/kitaev/. http://online.kitp.ucsb.edu/online/entangled15/kitaev2/
131. V. Balasubramanian, B. Craps, M. Khramtsov, E. Shaghoulian, Submerging islands through thermalization. JHEP **10**, 048 (2021). https://doi.org/10.1007/JHEP10(2021)048. arXiv:2107.14746
132. G. Vidal, R.F. Werner, Computable measure of entanglement. Phys. Rev. A **65**, 032314 (2002). https://doi.org/10.1103/PhysRevA.65.032314. arXiv:quant-ph/0102117
133. B.M. Terhal, M. Horodecki, D.W. Leung, D.P. DiVincenzo, The entanglement of purification. J. Math. Phys. **43**, 4286–4298 (2002). https://doi.org/10.1063/1.1498001
134. M.B. Plenio, S. Virmani, An Introduction to entanglement measures. Quantum Inf. Comput. **7**, 1–51 (2007). arXiv:quant-ph/0504163
135. R. Horodecki, P. Horodecki, M. Horodecki, K. Horodecki, Quantum entanglement. Rev. Mod. Phys. **81**, 865–942 (2009). https://doi.org/10.1103/RevModPhys.81.865. arXiv:quant-ph/0702225
136. S. Dutta, T. Faulkner, A canonical purification for the entanglement wedge cross-section. JHEP **03**, 178 (2021). https://doi.org/10.1007/JHEP03(2021)178. arXiv:1905.00577
137. P. Hayden, M. Lemm, J. Sorce, Reflected entropy is not a correlation measure. arXiv:2302.10208
138. P. Calabrese, J. Cardy, E. Tonni, Entanglement negativity in quantum field theory. Phys. Rev. Lett. **109**, 130502 (2012). https://doi.org/10.1103/PhysRevLett.109.130502. arXiv:1206.3092
139. P. Calabrese, J. Cardy, E. Tonni, Entanglement negativity in extended systems: a field theoretical approach. J. Stat. Mech. **1302**, P02008 (2013). https://doi.org/10.1088/1742-5468/2013/02/P02008. arXiv:1210.5359
140. P. Calabrese, J. Cardy, E. Tonni, Finite temperature entanglement negativity in conformal field theory. J. Phys. A **48**, 015006 (2015). https://doi.org/10.1088/1751-8113/48/1/015006. arXiv:1408.3043
141. H. Hirai, K. Tamaoka, T. Yokoya, Towards entanglement of purification for conformal field theories. PTEP **2018**, 063B03 (2018). https://doi.org/10.1093/ptep/pty063. arXiv:1803.10539
142. P. Caputa, M. Miyaji, T. Takayanagi, K. Umemoto, Holographic entanglement of purification from conformal field theories. Phys. Rev. Lett. **122**, 111601 (2019). https://doi.org/10.1103/PhysRevLett.122.111601. arXiv:1812.05268
143. M. Rangamani, M. Rota, Comments on entanglement negativity in holographic field theories. JHEP **10**, 060 (2014). https://doi.org/10.1007/JHEP10(2014)060. arXiv:1406.6989

144. P. Chaturvedi, V. Malvimat, G. Sengupta, Holographic quantum entanglement negativity. JHEP **05**, 172 (2018). https://doi.org/10.1007/JHEP05(2018)172. arXiv:1609.06609
145. P. Chaturvedi, V. Malvimat, G. Sengupta, Entanglement negativity, holography and black holes. Eur. Phys. J. C **78**, 499 (2018). https://doi.org/10.1140/epjc/s10052-018-5969-8. arXiv:1602.01147
146. P. Jain, V. Malvimat, S. Mondal, G. Sengupta, Holographic entanglement negativity conjecture for adjacent intervals in AdS_3/CFT_2. Phys. Lett. B **793**, 104–109 (2019). https://doi.org/10.1016/j.physletb.2019.04.037. arXiv:1707.08293
147. T. Takayanagi, K. Umemoto, Entanglement of purification through holographic duality. Nat. Phys. **14**, 573–577 (2018). https://doi.org/10.1038/s41567-018-0075-2. arXiv:1708.09393
148. V. Malvimat, S. Mondal, B. Paul, G. Sengupta, Holographic entanglement negativity for disjoint intervals in AdS_3/CFT_2. Eur. Phys. J. C **79**, 191 (2019). https://doi.org/10.1140/epjc/s10052-019-6693-8. arXiv:1810.08015
149. V. Malvimat, S. Mondal, B. Paul, G. Sengupta, Covariant holographic entanglement negativity for disjoint intervals in AdS_3/CFT_2. Eur. Phys. J. C **79**, 514 (2019). https://doi.org/10.1140/epjc/s10052-019-7032-9. arXiv:1812.03117
150. J. Kudler-Flam, S. Ryu, Entanglement negativity and minimal entanglement wedge cross sections in holographic theories. Phys. Rev. D **99**, 106014 (2019). https://doi.org/10.1103/PhysRevD.99.106014. arXiv:1808.00446
151. Y. Kusuki, J. Kudler-Flam, S. Ryu, Derivation of holographic negativity in AdS_3/CFT_2. Phys. Rev. Lett. **123**, 131603 (2019). https://doi.org/10.1103/PhysRevLett.123.131603. arXiv:1907.07824
152. J. Kumar Basak, V. Malvimat, H. Parihar, B. Paul, G. Sengupta, On minimal entanglement wedge cross section for holographic entanglement negativity. arXiv:2002.10272
153. J. Kumar Basak, H. Parihar, B. Paul, G. Sengupta, Covariant holographic negativity from the entanglement wedge in AdS_3/CFT_2. arXiv:2102.05676
154. X. Dong, X.-L. Qi, M. Walter, Holographic entanglement negativity and replica symmetry breaking. JHEP **06**, 024 (2021). https://doi.org/10.1007/JHEP06(2021)024. arXiv:2101.11029
155. D. Basu, A. Chandra, H. Parihar, G. Sengupta, Entanglement negativity in flat holography. SciPost Phys. **12**, 074 (2022). https://doi.org/10.21468/SciPostPhys.12.2.074. arXiv:2102.05685
156. D. Basu, A. Chandra, V. Raj, G. Sengupta, Entanglement wedge in flat holography and entanglement negativity. SciPost Phys. Core **5**, 013 (2022). https://doi.org/10.21468/SciPostPhysCore.5.1.013. arXiv:2106.14896
157. D. Basu, H. Parihar, V. Raj, G. Sengupta, Entanglement negativity, reflected entropy, and anomalous gravitation. Phys. Rev. D **105**, 086013 (2022). https://doi.org/10.1103/PhysRevD.105.086013. arXiv:2202.00683
158. M. Afrasiar, J. Kumar Basak, A. Chandra, G. Sengupta, Islands for entanglement negativity in communicating black holes. arXiv:2205.07903
159. M.J. Vasli, M.R. Mohammadi Mozaffar, K. Babaei Velni, M. Sahraei, Holographic study of reflected entropy in anisotropic theories. Phys. Rev. D **107**, 026012 (2023). https://doi.org/10.1103/PhysRevD.107.026012. arXiv:2207.14169
160. K. Babaei Velni, M.R. Mohammadi Mozaffar, M.H. Vahidinia, Some aspects of entanglement wedge cross-section. JHEP **05**, 200 (2019). https://doi.org/10.1007/JHEP05(2019)200. arXiv:1903.08490
161. M. Sahraei, M.J. Vasli, M.R.M. Mozaffar, K.B. Velni, Entanglement wedge cross section in holographic excited states. JHEP **08**, 038 (2021). https://doi.org/10.1007/JHEP08(2021)038. arXiv:2105.12476
162. K. Babaei Velni, M.R. Mohammadi Mozaffar, M.H. Vahidinia, Evolution of entanglement wedge cross section following a global quench. JHEP **08**, 129 (2020). https://doi.org/10.1007/JHEP08(2020)129. arXiv:2005.05673
163. M. Ghodrati, Encoded information of mixed correlations: the views from one dimension higher. arXiv:2209.04548
164. J. Basak Kumar, D. Basu, V. Malvimat, H. Parihar, G. Sengupta, Reflected entropy and entanglement negativity for holographic moving mirrors. JHEP **09**, 089 (2022). https://doi.org/10.1007/JHEP09(2022)089. arXiv:2204.06015
165. J.K. Basak, H. Chourasiya, V. Raj, G. Sengupta, Reflected entropy in Galilean conformal field theories and flat holography. Eur. Phys. J. C **82**, 1169 (2022). https://doi.org/10.1140/epjc/s10052-022-11129-8. arXiv:2202.01201
166. P. Hayden, O. Parrikar, J. Sorce, The Markov gap for geometric reflected entropy. JHEP **10**, 047 (2021). https://doi.org/10.1007/JHEP10(2021)047. arXiv:2107.00009
167. P. Bueno, H. Casini, Reflected entropy for free scalars. JHEP **11**, 148 (2020). https://doi.org/10.1007/JHEP11(2020)148. arXiv:2008.11373
168. H.A. Camargo, L. Hackl, M.P. Heller, A. Jahn, B. Windt, Long distance entanglement of purification and reflected entropy in conformal field theory. Phys. Rev. Lett. **127**, 141604 (2021). https://doi.org/10.1103/PhysRevLett.127.141604. arXiv:2102.00013
169. P. Bueno, H. Casini, Reflected entropy, symmetries and free fermions. JHEP **05**, 103 (2020). https://doi.org/10.1007/JHEP05(2020)103. arXiv:2003.09546
170. H.-S. Jeong, K.-Y. Kim, M. Nishida, Reflected entropy and entanglement wedge cross section with the first order correction. JHEP **12**, 170 (2019). https://doi.org/10.1007/JHEP12(2019)170. arXiv:1909.02806
171. Y. Kusuki, K. Tamaoka, Entanglement wedge cross section from CFT: dynamics of local operator quench. JHEP **02**, 017 (2020). https://doi.org/10.1007/JHEP02(2020)017. arXiv:1909.06790
172. D. Petz, Sufficient subalgebras and the relative entropy of states of a von Neumann algebra. Commun. Math. Phys. **105**, 123–131 (1986). https://doi.org/10.1007/BF01212345
173. O. Fawzi, R. Renner, Quantum conditional mutual information and approximate Markov chains. Commun. Math. Phys. **340**, 575–611 (2015). https://doi.org/10.1007/s00220-015-2466-x
174. T. Hartman, J. Maldacena, Time evolution of entanglement entropy from black hole interiors. JHEP **05**, 014 (2013). https://doi.org/10.1007/JHEP05(2013)014. arXiv:1303.1080
175. Y. Shao, M.-K. Yuan, Y. Zhou, Entanglement negativity and defect extremal surface. arXiv:2206.05951
176. J.D. Brown, M. Henneaux, Central charges in the canonical realization of asymptotic symmetries: an example from three-dimensional gravity. Commun. Math. Phys. **104**, 207–226 (1986). https://doi.org/10.1007/BF01211590
177. Y. Lu, J. Lin, The Markov gap in the presence of islands. arXiv:2211.06886
178. M. Afrasiar, J.K. Basak, A. Chandra, G. Sengupta, Reflected entropy for communicating black holes I: Karch-Randall Braneworlds. arXiv:2211.13246